Journal of Magnetic Resonance **147,** 192–209 (2000)
doi:10.1006/jmre.2000.2192, available online at http://www.idealibrary.com on IDEAL®

Population and Coherence Transfer Induced by Double Frequency Sweeps in Half-Integer Quadrupolar Spin Systems

Dinu Iuga, Hartmut Schäfer, Rieko Verhagen, and Arno P. M. Kentgens[1]

NWO/CW HF-NMR Facility, NSR Center, Toernooiveld 1, 6525 ED Nijmegen, The Netherlands

Received March 23, 2000; revised August 11, 2000

We have recently shown that the sensitivity of single- and multiple-quantum NMR experiments of half-integer ($N/2$) quadrupolar nuclei can be increased significantly by introducing so-called double frequency sweeps (DFS) in various pulse schemes. These sweeps consist of two sidebands generated by an amplitude modulation of the RF carrier. Using a time-dependent amplitude modulation the sidebands can be swept through a certain frequency range. Inspired by the work of Vega and Naor (*J. Chem. Phys.* 75, 75 (1981)), this is used to manipulate $\pm(m-1) \leftrightarrow \pm m$ ($3/2 \leq m \leq N/2$) satellite transitions in half-integer spin systems simultaneously. For ^{23}Na ($I = 3/2$) and ^{27}Al ($I = 5/2$) spins in single crystals it proved possible to transfer the populations of the outer $\pm m$ spin levels to the inner $\pm 1/2$ spin levels. A detailed analysis shows that the efficiency of this process is a function of the adiabaticity with which the various spin transitions are passed during the sweep. In powders these sweep parameters have to be optimized to satisfy the appropriate conditions for a maximum of spins in the powder distribution. The effects of sweep rate, sweep range, and RF field strength are investigated both numerically and experimentally. Using a DFS as a preparation period leads to significantly enhanced central transition powder spectra under both static and MAS conditions, compared to single pulse excitation. DFSs prove to be very efficient tools not only for population transfer, but also for coherence transfer. This can be exploited for the multiple- to single-quantum transfer in MQMAS experiments. It is demonstrated, theoretically and experimentally, that DFSs are capable of transferring both quintuple-quantum and triple-quantum coherence into single-quantum coherence in $I = 5/2$ spin systems. This leads to a significant enhancement in signal-to-noise ratio and strongly reduces the RF power requirement compared to pulsed MQMAS experiments, thus extending their applicability. This is demonstrated by ^{27}Al 3QMAS experiments on $9Al_2O_3 \cdot 2B_2O_3$ and the mineral andalusite. In the latter compound, Al experiences a quadrupolar-coupling constant of 15.3 MHz in one of the sites. Finally a 5QMAS spectrum on $9Al_2O_3 \cdot 2B_2O_3$ demonstrates the sensitivity enhancement of this experiment using a double frequency sweep.

Key Words: **MQMAS; double frequency sweeps; population transfer; coherence transfer; sensitivity enhancement.**

INTRODUCTION

The application of NMR to half-integer quadrupolar nuclei in powder samples has increased steadily since the early eighties. Nuclei possessing a quadrupole moment are common, some of the most important being ^{27}Al, ^{23}Na, and ^{17}O. They are encountered in catalysis, geochemistry, materials science, biomembranes, etc. Beside the chemical shift, NMR experiments of quadrupolar nuclei can provide the quadrupole coupling constant (C_{qcc}) and asymmetry parameter (η) of the electric field gradient tensor at the site of the nucleus. This information can, in principle, be obtained from the powder lineshape of the central transition in static or magic angle spinning (MAS) spectra of polycrystalline samples. The anisotropic contributions of the quadrupole interaction in MAS spectra are a source of information, but obviously compromise the resolution of the spectra. Therefore, important efforts were made to design experiments to increase the resolution of NMR spectra of these nuclei, while maintaining their information content. By far the most successful in this respect is the multiple-quantum magic angles spinning (MQMAS) experiment introduced by Frydman and Harwood (*1*). By combining manipulations in spatial and spin space, this experiment succeeds in obtaining two-dimensional spectra that are free of anisotropic broadening in one dimension while maintaining the anisotropic information in the other dimension. This is achieved by exciting $-m \leftrightarrow +m$ multiple-quantum coherences, which evolve during the evolution period of the experiment and a subsequent conversion into observable single-quantum coherence of the central $-1/2 \leftrightarrow +1/2$ transition. Due to the fact that, under MAS, these coherences evolve under identical fourth-rank spatial functions, albeit with different scalar scaling factors, a refocusing of the anisotropic terms occurs at a specific time during the acquisition period. Depending on the scaling factors an appropriate shearing of the spectra is necessary to obtain isotropic–anisotropic spectra, allowing the identification of different sites and accessing their quadrupolar parameters. 3QMAS spectra are sheared by a factor $-7/9$ for $I = 3/2$ spins and 19/12 for $I = 5/2$ spins. It is safe to say that by now the MQMAS experiment has evolved into a routine experiment which has found application in the study of

[1] To whom correspondence should be addressed. Fax: +31-24-3652112. E-mail: arno@solidmr.kun.nl.

1090-7807/00 $35.00

a wealth of crystalline and glassy materials. Unfortunately, the behavior of the quadrupolar nuclei in the MQMAS experiment strongly depends on the ratio of their quadrupolar frequency (Ω_Q) and the RF field strength (ω_1). Therefore, the multiple-quantum excitation and the multiple- to single-quantum coherence transfer must be carefully analyzed for quantitative interpretation of MQ spectra. Apart from this complication, the problem remains that the MQMAS experiment is rather insensitive and has problems with detecting sites with either very low or high C_{qcc} values. It is therefore not surprising that considerable efforts to improve the efficiency of the experiment were reported (*2–20*). A brute force approach is to increase the RF power to match large quadrupolar interactions. Although great progress was achieved in this approach by the spectrometer companies, this route remains limited. Other approaches rely on modulated pulses (*16–18*). Adiabatic passages hold great promise for the interconversion of multiple- and single-quantum coherence (*19, 20*). Based on the work of Vega (*21*) describing zero passages of the quadrupolar frequency in spinning samples in terms of adiabaticity considerations, Griffin and co-workers (*4*) introduced the RIACT sequence using CW pulses of a quarter rotor period. This technique relies on the adiabaticity of the quadrupolar zero crossings, which can only be influenced by the experimenter by changing the spinning speed, thus leaving a limited application window. Moreover, as was described by Vega and co-workers (*20, 22*), there are some more fundamental problems with the conversion as during the zero passage all energy levels are coupled.

The development of pulse modulation has a strong tradition. Nowadays, high-resolution NMR of spin-$\frac{1}{2}$ nuclei heavily relies on the use of phase and amplitude modulated sequences. The use of amplitude modulated pulses on half-integer quadrupolar spin systems was pioneered by Vega and Naor (*23*). For spin-3/2 systems in single crystals they showed that the central transition intensity could be increased by a factor of 3 by a combination of selective 90° pulses and amplitude modulated pulses that act as simultaneous 180° pulse on the satellite transitions. This concept of rearranging populations in a half-integer quadrupolar spin system to enhance the sensitivity is very attractive. To achieve this in powders, a pulsed approach fails as the satellite transitions cover a large frequency range from 0 to $\pm\omega_Q$. As was shown in a number of publications, adiabatic techniques form an attractive alternative (*24–28*). Our approach is to use frequency- or time-dependent amplitude modulation of the RF carrier to generate single and double frequency sweeps, which make it possible to invert one or both satellites for most crystallites in the powder distribution (*19*).

A further concept introduced by Vega and Naor (*23*) is the transfer of coherences in a quadrupolar spin system. Based on these ideas two new schemes were put forward to enhance MQMAS spectroscopy. Our procedure is a double frequency sweep (DFS) covering a frequency range affecting all satellite transitions in a powder (*19*). These DFSs are implemented using an external waveform generator that allows a pure amplitude modulation of the RF carrier. The second method, called FAM (fast amplitude modulation), was put forward by Vega and co-workers. In this scheme, which is of similar nature as the DFS, shifting the pulse phases alternatively by 180° creates a constant "amplitude" modulation. This method relies on magic angle spinning for most crystallites to adiabatically pass through the resonance conditions imposed by the fixed modulation frequency (*20, 22*). With both techniques signal gains of several factors and improved lineshapes were reported in 3QMAS spectra of spin-3/2 systems.

In this paper double frequency sweeps are studied in more detail to deepen our insight in the dynamics of quadrupolar spin systems with the goal to transfer populations or coherences. Population and coherence transfer, using amplitude modulated pulses, is studied both theoretically and experimentally in single crystals and powders. The application of the DFS to $I = 3/2$ and $5/2$ spin systems is demonstrated. Besides population transfer, the transfer of both quintuple- and triple-quantum coherence to single-quantum coherence will be investigated for $I = 5/2$. Finally the implementation of these methods in 3QMAS and 5QMAS experiments of the mineral andalusite, a compound with overall composition $2Al_2O_3 \cdot 2La_2O_3 \cdot 4B_2O_3$ treated at 1100°C, and crystalline $9Al_2O_3 \cdot 2B_2O_3$ is shown.

THEORETICAL DESCRIPTION

Modulated Spin-Hamiltonian

Half-integer quadrupolar nuclei with spin $I = N/2$ have $N + 1$ equidistant energy levels, due to the Zeeman interaction, when placed in a high external magnetic field. This allows for N single-quantum transitions. Depending on their surroundings the nuclei experience a quadrupolar interaction. In many practical cases this is an order of a magnitude smaller than the Zeeman interaction and can therefore be treated as a perturbation. In that case all energy levels are shifted by the quadrupolar interaction in first order; every energy level $\pm m$ is shifted by the same amount. As a result all $+m \leftrightarrow -m$ transitions, including the central transition, are not affected in first order. The effect is that the NMR spectrum of a half-integer quadrupolar nucleus consists of a line at the Zeeman frequency (i.e., the isotropic chemical shift) of the central transition, accompanied by a set of lines due to the satellite transitions $\pm(m - 1) \leftrightarrow \pm m$ $(3/2 \le m \le N/2)$ which are symmetrically displaced away from the central transition by n times ($n = \pm 1, \pm 2, \ldots$, for $m = 3/2, 5/2, \ldots$, etc.) the quadrupole frequency Ω_Q. The $N + 1$ energy levels are populated according to the Boltzmann distribution, which in the high-temperature approximation is proportional to I_z. It is of interest to have the possibility of redistributing the populations over the spin system, e.g., to bring the populations of the outer $\pm N/2$ levels

to the inner $\pm 1/2$ levels in order to increase the intensity of the central transition by a factor N.

To gain insight in these processes we have to study the dynamics of the spin system under appropriate RF irradiation. In first-order perturbation theory, the spin-Hamiltonian for quadrupolar nuclei with spin I in a high magnetic field under RF irradiation is given by

$$H = \Delta\omega I_z + \frac{1}{6}\,\Omega_Q[3I_z^2 - I(I+1)] + \omega_1 I_x \qquad [1]$$

in the rotating frame. Here

$$\Omega_Q(\theta, \varphi) = \frac{1}{2}\,\omega_Q(3\cos^2\theta - 1 + \eta\sin^2\theta\cos 2\varphi), \qquad [2]$$

$$\omega_Q = 2\pi\,\frac{3C_{qcc}}{2I(2I-1)}, \qquad [3]$$

and θ, φ are the polar angels orienting the external magnetic field in the principal axis system of the electric field gradient tensor. Here we will restrict ourselves to half-integer quadrupolar spins and leave dipolar interactions out of consideration. A further restriction of the theoretical analysis presented here is that we assume that $\omega_1 \ll \Omega_Q$ so that at most one transition is at resonance at a given offset or, in the case of modulated pulses, the simultaneous resonances of the satellite transitions are completely uncoupled. In this approach each transition can be described in their particular subspaces, e.g., using the fictitious spin-$\frac{1}{2}$ concept (*29, 30*).

A set of satellite transitions $\pm(m-1) \leftrightarrow \pm m$ can be inverted by an amplitude modulation of the RF field. It is well known that amplitude modulation of a carrier wave leads to sidebands. For a cosine modulation of the carrier with constant modulation frequency ω_m the RF Hamiltonian is given by

$$H_1 = \omega_1\cos(\omega_m t)I_x. \qquad [4]$$

As was explained by Vega and Naor (*23*), using the fictitious spin approach, for $\omega_m = \Omega_Q$ and $1/2\sqrt{3}\ \omega_1 t = \pi$ this modulated pulse effectively acts as two simultaneous, selective 180° pulses on the first satellite transitions, thus inverting their populations, which is in line with the expectations based on the fact that the modulation generates two sidebands at $\pm\omega_m$ with respect to the carrier frequency.

The same effect can be obtained with an adiabatic sweep when the RF frequency is slowly swept through the satellite transitions. This is achieved by sweeping the frequency from a position sufficiently far above resonance to a frequency well below resonance or vice versa. To accomplish this for both satellites simultaneously, the amplitude modulation frequency ω_m must be made time dependent. A great advantage of this approach is that the frequency range of the sweep can be chosen sufficiently large to cover the distribution in Ω_Q in powdered samples. The RF Hamiltonian in the rotating frame must now be written as

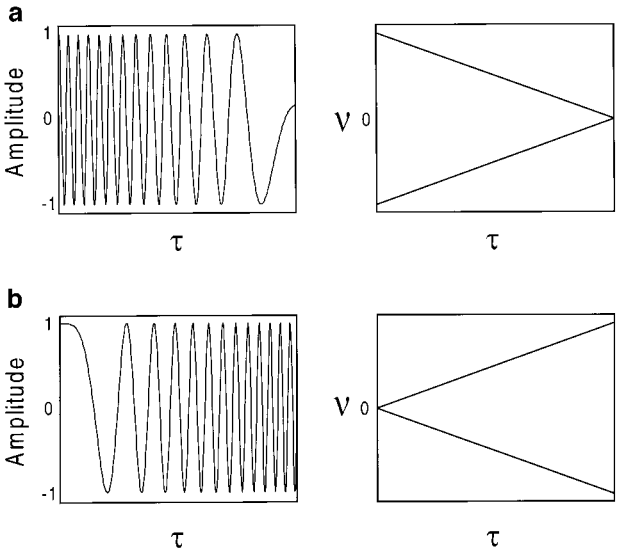

FIG. 1. Amplitude profiles for a converging (a) and diverging (b) double frequency sweep.

$$H_1(t) = \omega_1\cos\int_0^t \omega_m(t')dt' \cdot I_x. \qquad [5]$$

The time dependence of $\omega_m(t)$ can be chosen freely, e.g., to maintain constant adiabaticity for a transition (*31*). In powdered samples linear sweeps are preferred. In that case,

$$\omega_m(t) = \omega_s + \frac{(\omega_f - \omega_s)t}{\tau} \qquad [6]$$

sweeps the frequencies from starting frequency $\pm\omega_s$ to the final frequency $\pm\omega_f$ in a time τ (Fig. 1).

Implementation of the new RF Hamiltonian [5] makes the total Hamiltonian time dependent, which complicates an analytical treatment. The most insightful approach was introduced by Vega and colleagues (*20, 22, 23*). In this description the (on-resonance) Hamiltonian of a spin-3/2 system is described, using fictitious spin operators, by

$$H = \omega_Q(I_z^{1-2} - I_z^{3-4}) + (\sqrt{3}\ \omega_1(I_x^{1-2} + I_x^{3-4}) + 2\omega_1 I_x^{2-3})\cos\varphi(t) \qquad [7]$$

with

$$\varphi(t) = \int_0^t \omega_m(t')dt'. \quad [8]$$

To eliminate the time dependence in the RF term in the Hamiltonian a transformation into a modulation interaction frame, rotating with the instantaneous frequencies of the two sidebands, is brought about by the unitary operator

$$U(t) = T \cdot \exp\{-i\varphi(t) \cdot (I_z^{1-2} - I_z^{3-4})\}. \quad [9]$$

In the modulation interaction frame the Hamiltonian becomes

$$\begin{aligned} H = \Delta\omega_Q(I_z^{1-2} - I_z^{3-4}) + \sqrt{3}\ \omega_1\Big\{&\frac{1}{2}(I_x^{1-2} + I_x^{3-4}) \\ &\times [1 + \cos(2\varphi(t))] \\ &- \frac{1}{2}(I_y^{1-2} - I_y^{3-4})\sin(2\varphi(t))\Big\} \\ &+ 2\omega_1 I_x^{2-3}\cos(\varphi(t)), \end{aligned} \quad [10]$$

where

$$\Delta\omega_Q = \Omega_Q(t) - \omega_m(t). \quad [11]$$

For a nonspinning sample, Ω_Q is time independent. Under the assumption that $\omega_1 \ll \omega_m$, the terms containing $\varphi(t)$ represent oscillating terms and can therefore be neglected. In this way the only time dependence in the Hamiltonian [10] is in the I_z term.

For a spinning sample things are slightly more complicated as Ω_Q becomes time dependent. Supposing we start with a positive quadrupolar frequency, a passage through the satellites is reached at $\Omega_Q(t) = \omega_m(t)$ which can be described using the Hamiltonian [10] neglecting the oscillating terms. At a later point in time Ω_Q can become negative, however, and a further passage through resonance maybe encountered at $\Omega_Q(t) = -\omega_m(t)$. In this case we cannot discard the oscillating terms in [10], as they now are on-resonance. To arrive at a time-independent Hamiltonian for this transition the transformation into the modulation frame [9] should be carried out with a reversed sign of $\omega_m(t)$. An important consequence of the above description is that the Hamiltonian can be separated in pseudo spin-$\frac{1}{2}$ Hamiltonians for transitions 1–2 and 3–4, i.e., the two subspaces are uncoupled. A further important point to note is that the density matrix description of the 2–3 single- and 1–4 triple-quantum subspaces are left unaltered by the transformation in the modulation frame (*22*).

For 5/2 spins a similar approach can be used using the appropriate fictitious spin-1/2 operators; I_x becomes

$$I_x = \sqrt{5}\ (I_x^{1-2} + I_x^{5-6}) + 2\sqrt{2}\ (I_x^{2-3} + I_x^{4-5}) + 3I_x^{3-4} \quad [12]$$

and the quadrupolar Hamiltonian

$$H_Q = \Omega_Q\left[\frac{10}{3}(I_z^{1-2} - I_z^{5-6}) + \frac{8}{3}(I_z^{2-3} - I_z^{4-5})\right]. \quad [13]$$

Using the transformation

$$U(t) = \exp\left\{-i\varphi(t)\left[\frac{10}{3}(I_z^{1-2} - I_z^{5-6}) + \frac{8}{3}(I_z^{2-3} - I_z^{4-5})\right]\right\} \quad [14]$$

and discarding all oscillating terms, we end up with the Hamiltonian in the modulation frame

$$\begin{aligned} H = \Delta\omega_Q&\left[\frac{10}{3}(I_z^{1-2} - I_z^{5-6}) + \frac{8}{3}(I_z^{2-3} - I_z^{4-5})\right] \\ &+ \omega_1\sqrt{2}\ (I_x^{2-3} + I_x^{4-5}). \end{aligned} \quad [15]$$

From the Hamiltonian [15] we learn that if we modulate with a frequency close to $\pm\Omega_Q$ then the $I_x^{2-3} + I_x^{4-5}$ term is on-resonance and internal satellites are affected. Modulating at a frequency close $\pm 2\Omega_Q$, a similar approach as described above shows that the $I_x^{1-2} + I_x^{5-6}$ term becomes time independent and the quadrupolar term contains $\Delta\omega_Q = 2\Omega_Q(t) - \omega_m(t)$, meaning that the external satellites are affected. Therefore, with a linearly changing modulation frequency as given by Eq. [6], one can only affect the different sets of satellite transitions at different times. Again, ignoring offset effects, the Hamiltonian breaks down in various parts describing uncoupled subspaces.

Introducing resonance offsets in the Hamiltonian seriously complicates the analytical approach as the fictitious spin-Hamiltonian no longer breaks up in a sum of uncoupled sub-Hamiltonians. For an insightful discussion we therefore restrict ourselves to the on-resonance case. Moreover, the applications chosen in this contribution focus on nuclei with limited chemical shift ranges (^{23}Na and ^{27}Al) and as the experiments were performed in high external fields, second-order quadrupolar shifts, which can also be viewed as resonance offsets, are small. Therefore the effects of these terms are negligible in the present study. Madhu *et al.* (*22*) have shown the effects of resonance offsets for FAM conversion by numerical simulations. The effects of substantial resonance offsets encountered for nuclei with very large chemical shift ranges will need a separate study and possibly demand adaptation of linear DFS sweeps as defined by Eq. [6].

Population and Coherence Transfer during a Double Frequency Sweep

As described above, after discarding the oscillating terms, the ($I = 3/2$) Hamiltonian in the modulation frame

$$H = \Delta\omega_Q I_z^{1-2} + \frac{1}{2}\sqrt{3}\,\omega_1 I_x^{1-2} - \Delta\omega_Q I_z^{3-4} + \frac{1}{2}\sqrt{3}\,\omega_1 I_x^{3-4} \qquad [16]$$

consists of commuting terms that independently act on the spin system. These terms are identical to the subspace Hamiltonians derived in our description of single frequency sweeps in quadrupolar spin systems (*27*) except for the fact that the RF field strength is halved as the available field is equally distributed over the two RF sidebands. This means that it is possible to use double frequency sweeps to simultaneously invert the satellite transitions by an adiabatic passage in complete analogy with the description of single frequency sweeps presented before. Obviously in a single frequency sweep only one transition is inverted at a time.

In view of the suitability of the double frequency sweep for the conversion of triple- to single-quantum coherence, very similar conditions hold as for the conversion of populations in the spin system. The question is how the triple-quantum coherence terms $I_{x,y}^{1-4}$ in the density matrix evolve into single-quantum coherence terms $I_{x,y}^{2-3}$ under the Hamiltonian [16]. The analogy with population transfer becomes clear when a representation is chosen where coherences look like populations. This is achieved by the transformation (*22*)

$$U = \exp\left\{-i\,\frac{\pi}{2}\,I_y^{1-4}\right\}\exp\left\{i\,\frac{\pi}{2}\,I_y^{2-3}\right\}. \qquad [17]$$

Under this transformation $I_x^{1-4} \rightarrow I_z^{1-4}$, $I_x^{2-3} \rightarrow -I_z^{2-3}$ and the Hamiltonian [16] transforms into

$$H = \Delta\omega_Q I_z^{1-3} + \frac{1}{2}\sqrt{3}\,\omega_1 I_x^{1-3} - \Delta\omega_Q I_z^{2-4} - \frac{1}{2}\sqrt{3}\,\omega_1 I_x^{2-4}. \qquad [18]$$

This Hamiltonian describes two independent subspaces 1–3 and 2–4, so a full adiabatic passage will simultaneously invert the populations of $|1\rangle$ and $|3\rangle$ and of $|2\rangle$ and $|4\rangle$ in this tilted modulation frame. As a result, if we start with a density matrix consisting purely of triple-quantum coherence, this will be transferred to single-quantum coherence (*22*),

$$(I_x^{1-4})^{\mathrm{T}} = I_z^{1-4} = \begin{bmatrix} 1/2 & 0 & 0 & 0 \\ 0 & 0 & 0 & 0 \\ 0 & 0 & 0 & 0 \\ 0 & 0 & 0 & -1/2 \end{bmatrix} \xrightarrow{\text{adiabatic inversion of 1–3 and 2–4}}$$

$$\begin{bmatrix} 0 & 0 & 0 & 0 \\ 0 & -1/2 & 0 & 0 \\ 0 & 0 & 1/2 & 0 \\ 0 & 0 & 0 & 0 \end{bmatrix} = -I_z^{2-3} = (I_x^{2-3})^{\mathrm{T}}, \qquad [19]$$

similarly $I_y^{1-4} \rightarrow I_y^{2-3}$. There is no intermixing of x and y components as long as we ignore resonance offsets and second-order effects.

Similar considerations for spin 5/2 show that if we are close to resonance for the outer transitions we find the following Hamiltonian in the tilted rotating frame,

$$H = \Delta\omega_Q\left[\frac{10}{3}\,(I_z^{1-5} - I_z^{2-6}) + \frac{8}{3}\,(I_z^{2-4} - I_z^{3-5})\right] + \omega_1\,\frac{\sqrt{5}}{2}\,(I_x^{1-5} + I_x^{2-6}), \qquad [20]$$

with $\Delta\omega_Q = 2\Omega_Q(t) - \omega_m(t)$. Under this Hamiltonian the states $|2\rangle$ and $|6\rangle$, and $|1\rangle$ and $|5\rangle$, will be inverted during an adiabatic passage. This means that if we start with a density matrix consisting purely of quintuple-quantum coherence, this will be transferred to triple-quantum coherence,

$$(I_x^{1-6})^{\mathrm{T}} = I_z^{1-6} = \begin{bmatrix} \frac{1}{2} & 0 & 0 & 0 & 0 & 0 \\ 0 & 0 & 0 & 0 & 0 & 0 \\ 0 & 0 & 0 & 0 & 0 & 0 \\ 0 & 0 & 0 & 0 & 0 & 0 \\ 0 & 0 & 0 & 0 & 0 & 0 \\ 0 & 0 & 0 & 0 & 0 & -\frac{1}{2} \end{bmatrix} \xrightarrow{\text{adiabatic inversion of 1–5 and 2–6}}$$

$$\begin{bmatrix} 0 & 0 & 0 & 0 & 0 & 0 \\ 0 & -\frac{1}{2} & 0 & 0 & 0 & 0 \\ 0 & 0 & 0 & 0 & 0 & 0 \\ 0 & 0 & 0 & 0 & 0 & 0 \\ 0 & 0 & 0 & 0 & \frac{1}{2} & 0 \\ 0 & 0 & 0 & 0 & 0 & 0 \end{bmatrix} = -I_z^{2-5} = (I_x^{2-5})^{\mathrm{T}}. \qquad [21]$$

For modulation near the inner satellite transitions, the tilted frame Hamiltonian is

$$H = \Delta\omega_Q\left[\frac{10}{3}\,(I_z^{1-2} - I_z^{5-6}) + \frac{8}{3}\,(I_z^{2-4} - I_z^{3-5})\right] + \omega_1\sqrt{2}\,(I_x^{3-5} + I_x^{2-4}), \quad [22]$$

with $\Delta\omega_Q = \Omega_Q(t) - \omega_m(t)$, so that an adiabatic sweep around $\Delta\omega_Q = 0$ leads to a level anticrossing of levels $|2\rangle$ and $|4\rangle$, and $|3\rangle$ and $|5\rangle$. In this case triple-quantum coherence is transferred to single-quantum coherence,

$$(-I_x^{2-5})^T = I_z^{2-5} = \begin{bmatrix} 0 & 0 & 0 & 0 & 0 & 0 \\ 0 & \frac{1}{2} & 0 & 0 & 0 & 0 \\ 0 & 0 & 0 & 0 & 0 & 0 \\ 0 & 0 & 0 & 0 & 0 & 0 \\ 0 & 0 & 0 & 0 & -\frac{1}{2} & 0 \\ 0 & 0 & 0 & 0 & 0 & 0 \end{bmatrix} \xrightarrow{\text{adiabatic inversion of 2–4 and 3–5}} \begin{bmatrix} 0 & 0 & 0 & 0 & 0 & 0 \\ 0 & 0 & 0 & 0 & 0 & 0 \\ 0 & 0 & -\frac{1}{2} & 0 & 0 & 0 \\ 0 & 0 & 0 & \frac{1}{2} & 0 & 0 \\ 0 & 0 & 0 & 0 & 0 & 0 \\ 0 & 0 & 0 & 0 & 0 & 0 \end{bmatrix} = -I_z^{3-4} = (I_x^{3-4})^T. \quad [23]$$

Note that this is markedly different to the RIACT case where during a zero-crossing quintuple-quantum coherence is directly converted to single-quantum coherence and triple-quantum coherence is inverted. In the adiabatic limit no triple- to single-quantum coherence transfer takes place in the RIACT experiment (*21*).

Adiabaticity Considerations

The concept of adiabaticity has been described in the monograph of Abragam (*32*) for a spin 1/2. For spinning quadrupolar nuclei, Vega (*21*) has derived the adiabaticity conditions describing the zero-crossings of the quadrupolar frequency under on-resonance RF irradiation. The effects of frequency stepped adiabatic passages in half-integer quadrupolar nuclei were described by van Veenendaal *et al.* (*27*). A similar approach can be made for the amplitude modulated pulses that generate double frequency sweeps. As the subspaces for the satellite transitions are not coupled in the Hamiltonian, one can consider the individual transition 1–2 and 3–4 separately and analyze the adiabaticity of their transitions. Thus, in static systems the adiabaticity parameter describing the passage of the satellites is

$$A^{1-2} = A^{3-4} = \frac{\omega_{\text{eff}}^2}{\lambda} = \frac{3\omega_1^2}{4\lambda}, \quad [24]$$

where λ is the sweep rate for a linear sweep and ω_1 the RF field strength which gets distributed equally over the two sidebands in the sweep. For the double- and triple-quantum transition one should consider their effective coupling fields of 7/8 ω_1^2/Ω_Q and 3/16 ω_1^3/Ω_Q^2, respectively, as calculated by Wokaun and Ernst (*30*) and Vega (*29*). Again the distribution of the field over the two sidebands has been taken into account. To allow comparison with our previous work, we characterize the adiabaticity of our double frequency sweeps with a single adiabaticity parameter

$$A = \frac{\omega_1^2}{4\lambda}, \quad [25]$$

which describes the on-resonance adiabaticity of a single sideband (cf. Eq. [10] in (*27*)).

In general we will be dealing with powdered samples and therefore the distribution in Ω_Q has to be taken into account. Ideally one wants to traverse the single-quantum transitions for polarization or coherence transfer adiabatically and all other transitions suddenly for every orientation in the powder. In practice this is not possible; the sweeps have to be optimized to fulfill the desired condition for as many crystallites in the powder as possible. As mentioned before, this is completely analogous to the discussion of single-frequency sweeps described before (*27*).

In the case of magic angle spinning an extra complication arises, as the quadrupolar frequency Ω_Q of each spin packet will become time-dependent (*33*):

$$\Omega_Q(t) = \frac{\omega_Q}{2}\,[A_1\cos(\omega_r t + \gamma) + A_2\sin(\omega_r t + \gamma) + B_1\cos(2\omega_r t + 2\gamma) + B_2\sin(2\omega_r t + 2\gamma)] \quad [26]$$

$$A_1 = \frac{\sqrt{2}\,\sin\varphi\cos\varphi(\eta\cos 2\theta - 3)}{3}$$

$$A_2 = -\frac{\sqrt{2}\,\eta\,\sin\varphi\sin 2\theta}{3}$$

$$B_1 = \frac{\frac{3}{2}\sin^2\varphi + \frac{1}{2}\,\eta\cos^2 2\theta(1 - \cos^2\varphi)}{3}$$

$$B_2 = -\frac{\eta\cos\varphi\sin 2\theta}{3}.$$

In the case of on-resonance CW irradiation the zero-crossings of $\Omega_Q(t)$ can be described as a sweep through various transi-

tions, leading to (partially) adiabatic processes in the spin system. This was extensively described by Vega (*21*) and is the basis of the RIACT phenomenon. If a frequency sweep is applied to a rotating sample, a more complicated situation occurs as both the RF frequency and the quadrupolar frequency are time-dependent. For the double frequency sweep described in the modulation frame the rate of change of the quadrupolar term $\Delta\omega_Q(t) = \Omega_Q(t) - \omega_m(t)$ through zero determines the adiabaticity of the transition:

$$A = \frac{\omega_{\text{eff}}^2}{\frac{d}{dt}\Delta\omega_Q(t)}. \qquad [27]$$

The rate of change of H_{eff} is now determined by the combined effect of spinning and frequency sweeping. As these terms can add or subtract nonadiabatic spinning and sweeping can still lead to an adiabatic passage and vice versa.

POPULATION TRANSFER

Static Single Crystal, Spin 3/2

For a single crystalline spin-3/2 system, with the Zeeman and quadrupolar interactions as the main interactions, the populations of the energy levels are proportional to I_z in the high-temperature approximation. In order to increase the polarization for the central transition one can simultaneously invert the satellite transitions prior to the normal excitation and observation of the spectra. In this way the populations of the outer levels $|1\rangle$ and $|4\rangle$ are transferred to the inner levels $|2\rangle$ and $|3\rangle$, increasing their population difference by a factor of 3. A complete inversion of the satellites ($|1\rangle \leftrightarrow |2\rangle$ and $|3\rangle \leftrightarrow |4\rangle$, respectively) can be achieved by selective 180° pulses on these transitions (*23*) or by subsequent adiabatic frequency sweeps over these satellites (*26*). Single frequency sweeps generated by stepping the frequency phase continuously have been analyzed in great detail (*27*). For the description of these sweeps it is useful to transform into a rotating frame that rotates with the instantaneous frequency of the RF field. In this frame, for the case where $\omega_1 \ll \Omega_Q$, the energy level diagram is depicted in Fig. 2a. During this sweep all transitions in the spin system are traversed one by one as indicated in the picture. In case of a double frequency sweep, generated with a time-dependent amplitude modulation [5], both satellites can be inverted simultaneously. Figure 2b shows the energy level diagram during a DFS defined in Eq. [6] in the modulation interaction frame. In this frame the external levels $|1\rangle$ and $|4\rangle$ and the internal levels $|2\rangle$ and $|3\rangle$ are degenerate. If the DFS is slow enough both satellite transitions $|1\rangle \leftrightarrow |2\rangle$ and $|3\rangle \leftrightarrow |4\rangle$ will experience an adiabatic level anticrossing and will be inverted.

In order to analyze the response of the spin system subjected to a DFS, we must solve the equation of motion under the Hamiltonian [7]. For the idealized situation $\omega_1 \ll \Omega_Q$ the

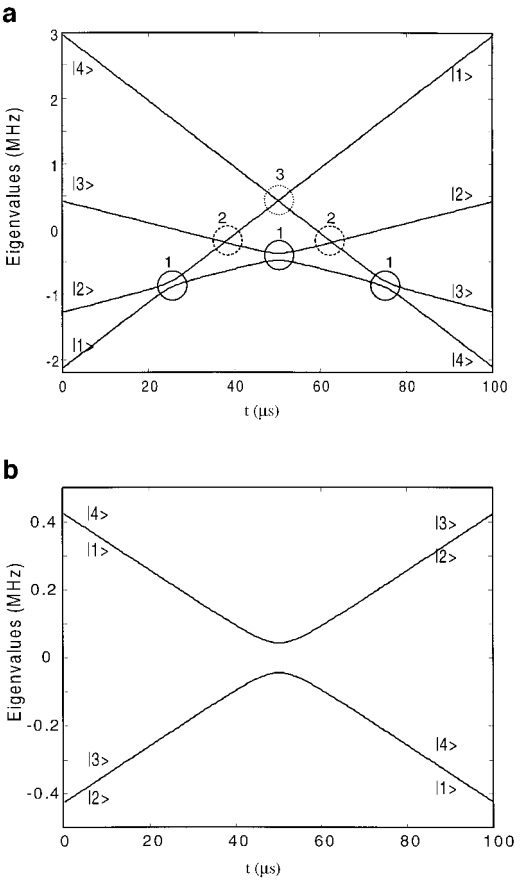

FIG. 2. Energy level diagrams for an $I = 3/2$ spin with $\Omega_Q/2\pi = 850$ kHz. (a) Linear single frequency sweep from -1.3 to $+1.3$ MHz in 100 μs ($\nu_1 = 50$ kHz) represented in the rotating frame. (b) Double frequency sweep from 0 to ± 1.3 MHz in 100 μs ($\nu_1 = 50$ kHz), represented in the modulation interaction frame defined by Eq. [9].

eigenvalues and functions of the Hamiltonian can be evaluated analytically. To cover all experimental conditions we choose a numerical approach, analyzing the time dependence by piecewise constant Hamiltonians. Figure 3 shows the influence of adiabaticity parameter on the inversion of the satellite transitions for a single crystal with $\Omega_Q/2\pi = 850$ kHz ($C_{qcc} = 1.7$ MHz). The DFS runs from $\nu_s = 0.4$ MHz to $\nu_f = 1.3$ MHz, using an RF field strength of 10 kHz. Figures 3a, 3b, and 3c show the time evolution of the level populations as viewed from the modulation interaction frame for DFSs with $A = 0.22$, 0.04, and 0.001, respectively. Figures 3d, 3e, and 3f show the same results as viewed from the laboratory frame. From Fig. 3a it is clear that even for an adiabaticity parameter as low as 0.22 ($A^{1-2} = A^{3-4} = 0.66$) the passage of the satellite transitions is completely adiabatic. As viewed from the modulation frame, this adiabatic behavior reveals itself in the absence of any change in the level populations, i.e., the spin system closely follows the change of the Hamiltonian. As was indicated in Fig. 2b, the eigenfunctions interchange their label during the course of the DFS. Therefore, if we monitor the

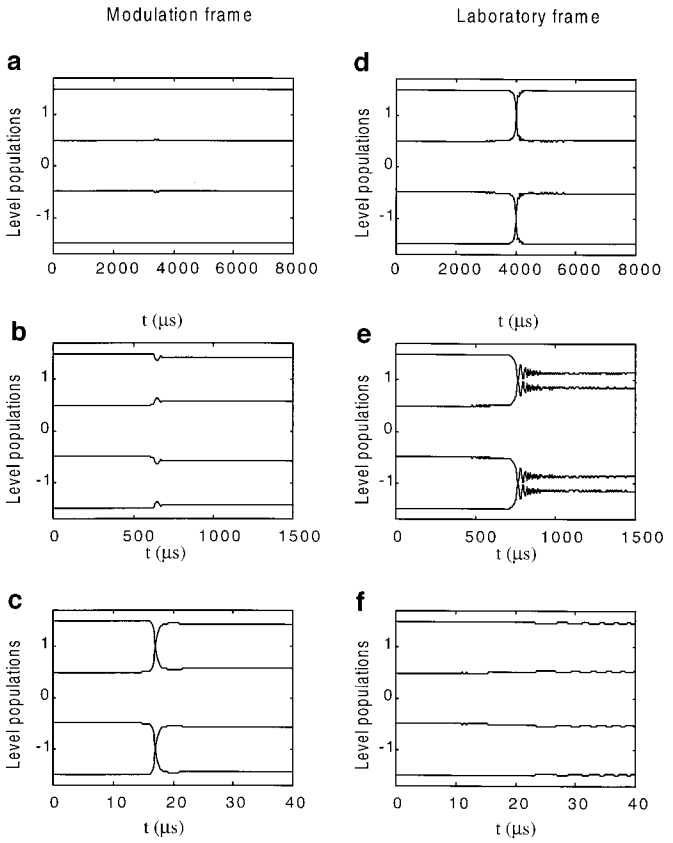

FIG. 3. Evolution of the level populations for a spin $I = 3/2$ ($\Omega_Q/2\pi =$ 850 kHz) during a DFS with $\nu_1 = 10$ kHz viewed from the modulation frame (a–c) or the laboratory frame (d–f). Adiabatic passages are realized for an overall sweep time of 8 ms (a and d, $A = 0.22$). Intermediate behavior is witnessed for a sweep time of 1.5 ms (b and e, $A = 0.04$), whereas the transitions are traversed suddenly for sweeps of 40 μs (c and f, $A = 0.001$).

process from the laboratory frame, an inversion of the level populations of the satellite transitions takes place (Fig. 3d). For a DFS characterized with an A of 0.04 (Figs. 3b and 3e) we observe intermediate behavior in terms of adiabaticity, with oscillations and partial equilibration of the level populations. For a very rapid sweep with an adiabaticity parameter of $A =$ 0.001 the passage of the satellite transitions is completely sudden. In the modulation frame we therefore see an interchange of the level populations (Fig. 3c). Translated to the laboratory frame this means that the spin system had no time to react to the applied field and all populations remain unchanged (Fig. 3f).

In our previous work (*19*) we demonstrated the effectiveness of the DFS for simultaneously inverting the satellite transitions for the ^{23}Na resonance in a single crystal of $NaNO_3$ ($C_{qcc} =$ 0.337 MHz, $\eta = 0$). We found that an appropriately chosen DFS applied before a selective 90° pulse excitation of the central transition led to an increase of the central transition intensity by a factor of 2.97, close to the theoretical maximum of 3. In order to further verify the adiabaticity of this process the central line intensity was monitored as a function of the sweep time, i.e., the adiabaticity of the sweeps. First a selective sweep over the satellite transitions was chosen; the DFS ranged from 60 to 100 kHz with the resonance position of the satellite transitions at $\pm$85 kHz. Figure 4 shows the intensity curves as a function of the overall sweep time at an RF field strength of $\sim$2 kHz ($\cdots$), 5 kHz ($\cdot-\cdot$), and 10 kHz ($---$). Clearly, the higher the RF field strength the sooner the transitions are traversed adiabatically as A is proportional to ω_1^2. At an RF field strength of $\sim$2 kHz the maximum signal intensity is still not reached using a sweep of 8 ms; at this point the adiabaticity of the sweep is 0.2. At 5 kHz a plateau is reached after about 2 ms corresponding to $A \sim 0.3$. At 10 kHz the maximum is reached at approximately 1 ms, followed by a slight decline in intensity. This is probably related to the fact that with the increased RF field we slightly violate the condition $\omega_1 \ll \Omega_Q$. If the sweep range is increased to run from 10 to 190 kHz, the double-quantum transitions of the spin system are traversed as well. A (partially) adiabatic passage of the 2Q transitions again depopulates the central levels and thus reverts the signal gain induced by the inversion of the satellites. This is visible in the solid curve ($\nu_1 = 12.5$ kHz) in Fig. 4, which shows a decreasing signal intensity with increasing sweep time. For these sweeps an optimum has to be found where the single-quantum transitions are traversed as adiabatically as possible, whereas the higher quantum transitions should be traversed as suddenly as possible. This optimum is found around $A \sim 0.15$ where the signal gain is still a factor of 2.5. This is in complete analogy with our work on single frequency sweeps (cf. Fig. 2e in (*27*)).

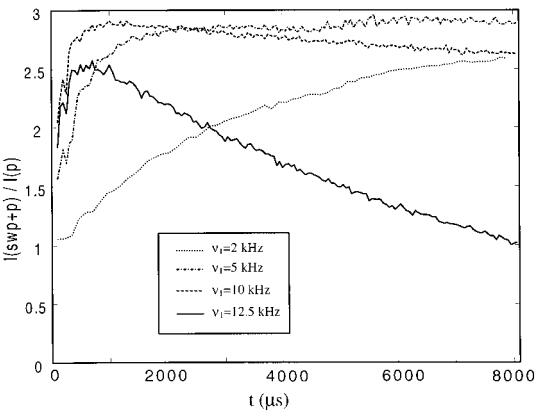

FIG. 4. Experimental intensity gain by applying DFSs of different RF field strengths (2 kHz ($\cdots$), 5 kHz ($\cdot-\cdot$), 10 kHz ($---$)) prior to a selective 90° pulse for the ^{23}Na resonance in a single crystal of $NaNO_3$ ($\Omega_Q/2\pi = 85$ kHz). The overall duration of the DFSs, running from 60 to 100 kHz, was varied. For the solid curve the sweep range was extended to 10–190 kHz so that the double-quantum transitions are traversed as well. The RF field strength was 12.5 kHz. A (partially) adiabatic passage of the 2Q transitions again depopulates the central levels and thus reverts the signal gain induced by the inversion of the satellites as is witnessed by a decrease in intensity with increasing sweep time. The maximum efficiency in this curve occurs at an adiabaticity factor $A \sim 0.15$.

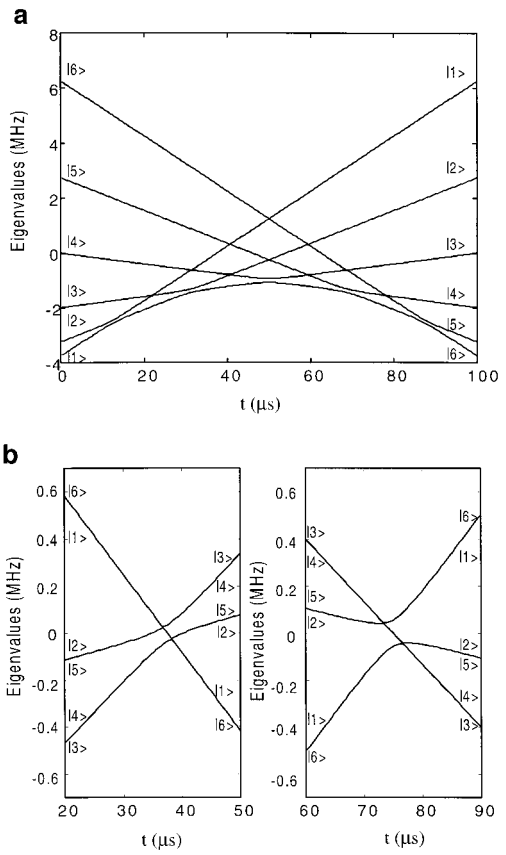

FIG. 5. Energy level diagrams for an $I = 5/2$ spin with $\Omega_Q/2\pi = 750$ kHz. (a) Linear single frequency sweep from -2 to $+2$ MHz in 100 μs ($\nu_1 = 50$ kHz) represented in the rotating frame. (b) Double frequency sweep from 0 to ± 2 MHz in 100 μs ($\nu_1 = 50$ kHz), represented in the respective modulation interaction frames for the inner and outer satellites.

Static Single Crystal, Spin 5/2

For $I = 5/2$ spins, similar considerations hold as for $I = 3/2$ spins, but more transitions are encountered. The energy diagrams for a linear sweep and a DFS are represented in Fig. 5. Note that during the linear sweep the single-quantum transitions occur successively. In the case of a DFS, represented in the modulation interaction frame in the fictitious spin-1/2 approach for irradiation near Ω_Q and $2\Omega_Q$ (Fig. 5b), we observe the simultaneous passage of the two inner satellites and the outer satellites, respectively.

Beside adiabaticity considerations the direction of the sweep is now of importance. For a diverging sweep the inner satellites are traversed before the outer satellites, whereas it is the other way around for a converging sweep. Figure 6 shows the effect on the level populations in the laboratory frame for a converging and diverging sweep of different length (i.e., adiabaticity). The numerical simulations were performed for a system with quadrupolar coupling constant $C_{qcc} = 5$ MHz ($\Omega_Q/2\pi = 750$ kHz, $2\Omega_Q/2\pi = 1.5$ MHz) for a DFS ranging from ± 2 to ± 0.4 MHz and vice versa. The rf field strength was 6 kHz and the sweep duration was 20 and 3 ms, leading to an adiabaticity parameter of $A = 0.11$ and 0.017, respectively. The converging DFS with $A = 0.11$ (Fig. 6a) displays nicely adiabatic passages of the (single-quantum) satellite transitions. First the populations of the $|1\rangle \leftrightarrow |2\rangle$ and $|5\rangle \leftrightarrow |6\rangle$ transitions are exchanged; subsequently the transitions $|2\rangle \leftrightarrow |3\rangle$ and $|4\rangle \leftrightarrow |5\rangle$ are inverted thus bringing the original populations of the outer levels $|1\rangle$ and $|6\rangle$ into the central levels $|3\rangle$ and $|4\rangle$, respectively. This means that the polarization in the central transition is increased by a factor of 5. For the diverging sweep (Fig. 6c) the inner satellites are traversed first so that the central transition will not be affected by the passage of the outer satellites. Therefore its polarization is increased by only a factor of 3. For faster sweeps the transitions are no longer traversed adiabatically and partial saturation takes place, as is shown for $A = 0.017$ in Figs. 6b and 6d.

To experimentally verify the analysis described above, we studied the ^{27}Al resonance in a single crystal of α-Al_2O_3 ($C_{qcc} = 2.38$ MHz, oriented such that $\Omega_Q/2\pi = 180$ kHz). Spectra obtained with a hard ($\nu_1 = 155$ kHz), respectively soft ($\nu_1 = 13$ kHz) excitation pulse are presented in Figs. 7a and 7b. Using the hard pulse excitation we observe five lines from the central line and the satellite transitions. A soft 90° pulse selectively excites the central transition only, so we observe one line (Fig. 7b). The intensity of this line serves as a reference. Next we employed an adiabatic ($A = 0.15$) DFS to manipulate the level populations prior to pulse excitation.

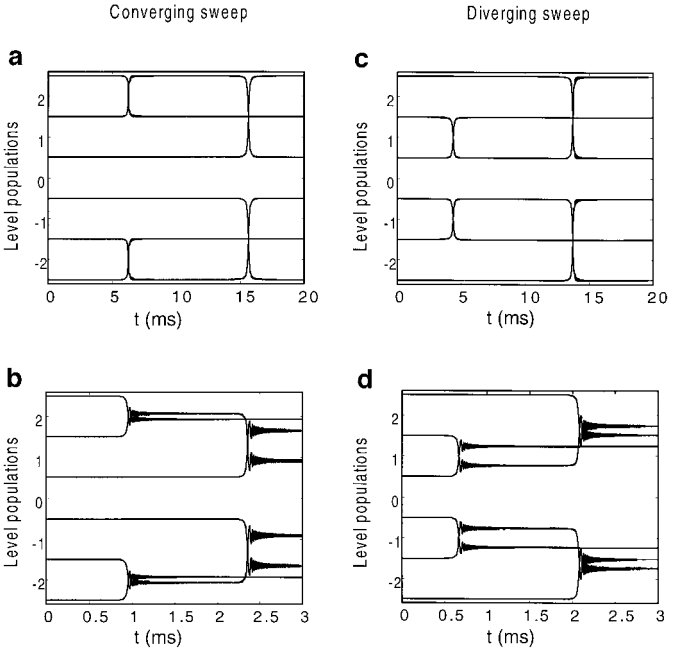

FIG. 6. Evolution of the level populations for a spin $I = 5/2$ ($\Omega_Q/2\pi = 750$ kHz) during a DFS with $\nu_1 = 6$ kHz viewed from the laboratory frame. The DFSs run from 0.4 to 2 MHz. (a) Converging sweep with $A = 0.11$; (b) converging sweep with $A = 0.017$; (c) diverging sweep with $A = 0.11$; (d) diverging sweep with $A = 0.017$.

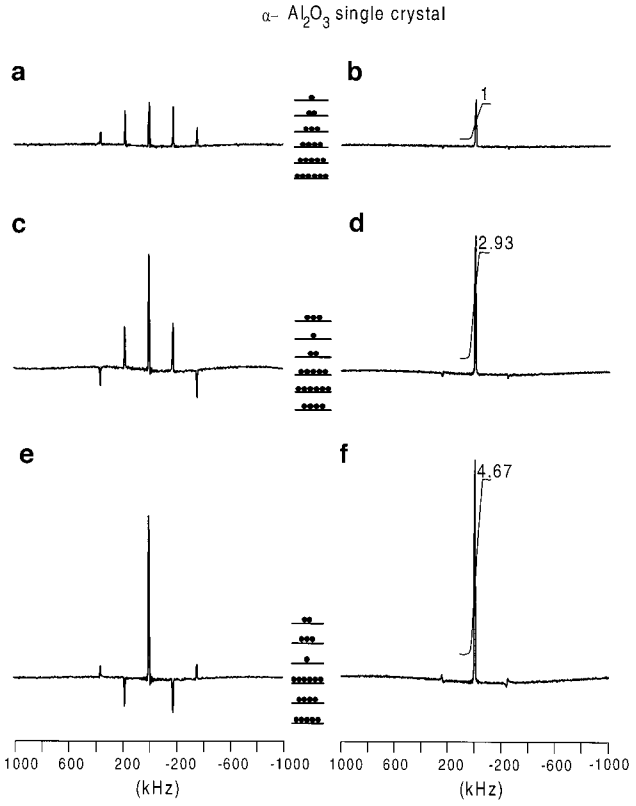

FIG. 7. (a) Hard pulse excitation ($\nu_1 = 155$ kHz) of ^{27}Al in a single crystal of a α-Al_2O_3 showing the central transition and four satellites. (b) Selective excitation ($\nu_1 = 13$ kHz) of the central transition. Diverging sweep ($A = 0.15$) followed by (c) a hard pulse and (d) a selective 90° pulse showing a signal gain close to 3. Converging sweep ($A = 0.15$) followed by (e) a hard pulse and (f) a soft pulse, now leading to a signal gain of approximately 5. The population distribution prior to the pulse excitation is indicated in the center.

Figure 7c shows the spectrum obtained by hard pulse excitation after a diverging DFS. The polarization of the inner satellites is positive and that of the outer satellites negative, in line with the expected state populations created by the diverging DFS. This sweep increases the signal intensity of the central transition after a selective excitation by a factor of 2.93, close to the theoretically achievable 3 (Fig. 7d). A converging DFS also leads to the expected results, followed by a hard pulse, negatively polarized inner satellites are observed next to positive outer satellites (Fig. 7e). Using a selective 90° pulse, the intensity of the central transition appears to be increased by a factor 4.67, close to the expected factor of 5.

An analysis of the adiabaticity can again be made by recording the central transition intensity as a function of the sweep time. In Fig. 8 the experimental gain is presented for α-Al_2O_3 ($\Omega_Q/2\pi = 180$ kHz) for sweeps with different RF field strength (3 kHz (a), 9 kHz (b), and 27 kHz (c)). For a converging sweep using a field of 3 kHz an increase of the central line intensity is observed with increasing sweep time. This is because the single-quantum satellite transitions are still not traversed fully adiabatically. At 9 kHz the maximum signal gain of 4.7 is reached already for sweeps of 2 ms and longer. At 27 kHz the maximum intensity is reached for very short sweeps followed by a decrease in intensity with increasing sweep time as the double-quantum transitions also start to be traversed more adiabatically, which is undesirable. For diverging sweeps, the 3- and 9-kHz sweeps have the same shape as those for the converging sweep, with the exception that the maximum signal gain is now close to 3, as only the inversion of the inner satellites brings a polarization gain for the central transition. An interesting phenomenon is observed for the 27-kHz curve, however. Instead of a decrease in intensity with increasing

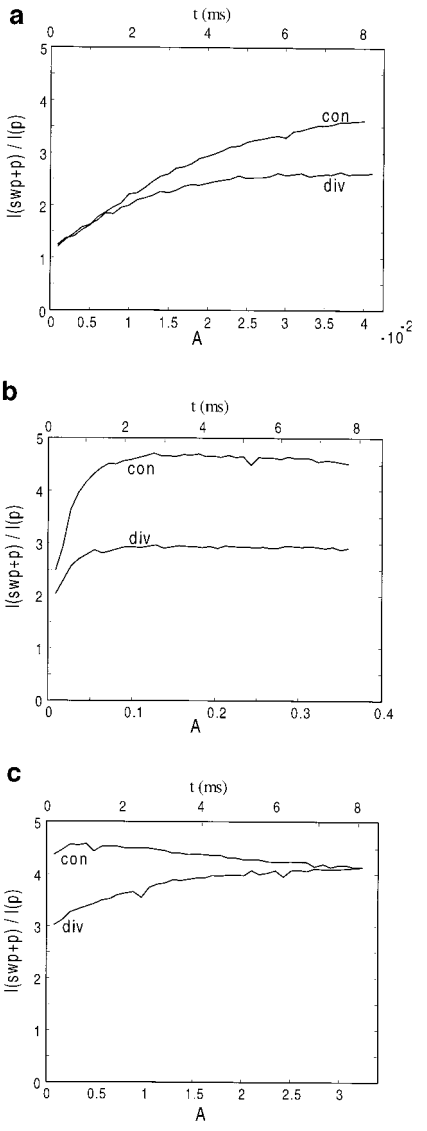

FIG. 8. Experimental intensity gain, by applying a DFSs of varying RF field strength prior to a selective 90° pulse, for the ^{27}Al resonance in a single crystal of α-Al_2O_3 ($\Omega_Q/2\pi = 180$ kHz). The overall duration of the DFSs, running from 100 to 550 kHz, was varied. The sweep duration is indicated at the top in milliseconds, whereas the adiabaticity parameter A is given on the lower x-axis. Converging and diverging sweeps are shown for ν_1 = (a) 3 kHz, (b) 9 kHz, and (c) 27 kHz.

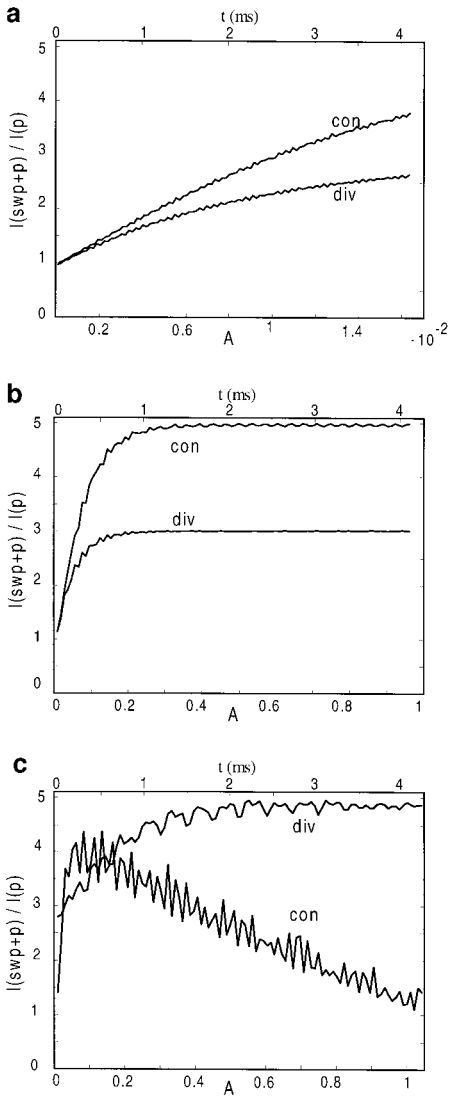

FIG. 9. Calculated intensity gains using converging and diverging DFS preparations, under idealized conditions for a spin $I = 5/2$ ($\Omega_Q/2\pi = 750$ kHz). ν_1 = (a) 6 kHz, (b) 46 kHz, and (c) 70 kHz.

sweep time, an increase above 3 is detected. For diverging sweeps an adiabatic passage of the $|1\rangle \leftrightarrow |3\rangle$ and $|4\rangle \leftrightarrow |6\rangle$ double-quantum transitions does convert the populations of the outermost levels to the inner levels. This is corroborated by numerical simulations (Fig. 9), which shows that a 500% increase in the polarization of the central line is possible for a diverging sweep if we cross the double-quantum transition fully adiabatically (Fig. 9c). Such a full adiabatic passage of the 2Q transitions is hardly realized in practice, however, as it needs extremely long sweeps or high RF field strength. By increasing the RF field strength one will soon violate the condition $\omega_1 \ll \Omega_Q$, in which case all transitions will be affected simultaneously and the concept of individual passages breaks down.

Powder Samples

Due to the orientational dependence of the quadrupole interaction, a distribution in Ω_Q, ranging from 0 to $\pm\omega_Q$, occurs in powder samples. For a fraction of the crystallites, the condition $\omega_1 \ll \Omega_Q$ that was assumed in our theoretical considerations will not be fulfilled. For these crystallites it is not possible to discuss adiabatic 1Q and sudden MQ transitions, as the transitions are not well separated. Numerical simulations have shown that the signal gain for these crystallites is not the full 300% for $I = 3/2$ or 500% for $I = 5/2$. The experimental signal gain as a function of sweep time for the ^{23}Na resonance in powdered $NaNO_2$ ($C_{qcc} = 1.1$ MHz, $\eta = 0.11$) is shown in Fig. 10a. Curves obtained at different RF field strengths were obtained for a DFS running from 0 to 750 kHz. After this DFS a selective 90° pulse was administered to the sample and the central transition spectrum was recorded. The response of the sample to a selective 90° pulse alone was used as a reference, i.e., intensity 1. We observe signal gains of approximately 230% in a nonspinning situation under optimum conditions. Spin-5/2 spins also behave completely as expected, as can be seen in Fig. 10b showing the response of the ^{27}Al signal in powdered α-Al_2O_3 ($C_{qcc} = 2.38$ MHz, $\eta = 0$) as a function of sweep time using converging and diverging DFSs of different rf field strengths. The maximum gain in these cases ends up at about 200% for a diverging sweep and 300% for a converging sweep. Again, the effect of crossing the double-quantum transitions partially adiabatically at higher RF field strength can be clearly distinguished by the decrease in intensity at increasing sweep times.

COHERENCE TRANSFER

Spin $I = 3/2$

The DFS performance for transferring populations in the spin system has been demonstrated convincingly so far. As was described in the theoretical introduction, the DFS should be equally effective in the conversion of triple- to single-quantum coherence. In the MQMAS experiment one wants to achieve an optimal conversion from $I_{x,y}^{1-4}$ to $I_{x,y}^{2-3}$, which as viewed from an appropriate modulation frame is similar to converting I_z^{1-4} to I_z^{2-3} population. This means that a simultaneous, selective 180° pulse on both satellite transitions should lead to a full transfer of triple- to single-quantum coherence. Vega and Naor demonstrated that this is indeed the case (*23*). To achieve the same effect in a powder a double frequency sweep over a large frequency range should be a superior alternative to pulsed inversion. We experimentally demonstrated the effectiveness of the DFS in this respect in a study of $I = 3/2$ spin systems in some model compounds (*19, 34*).

An in-depth evaluation of the theoretical concept was recently presented by Vega and co-workers (*22*) for adiabatic transfer using their fast amplitude modulation sequence which splits the excitation in two sidebands. As was discussed there

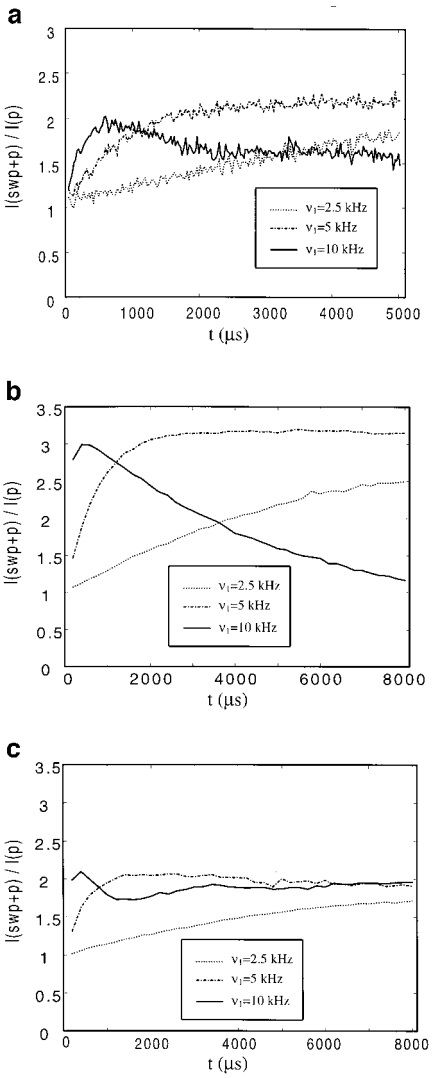

FIG. 10. Experimental intensity gain by applying DFSs of varying RF field strength prior to a selective 90° pulse for (a) the ^{23}Na ($I = 3/2$) resonance in powdered $NaNO_2$ ($\omega_Q = 550$ kHz) and (b, c) the ^{27}Al ($I = 5/2$) resonance in powdered α-Al_2O_3 ($\omega_Q = 357$ kHz). The sweeps in (a) run from 0 to ± 750 kHz. The sweeps in (b) run from ± 850 kHz to 0 and in (c) from 0 to ± 850 kHz. The RF fields are 2.5 kHz (· · ·), 5 kHz (· – ·), and 10 kHz (—).

and corroborated by our own work, the basic mechanism acting in FAM and DFS is identical, with the exception that the DFS has more degrees of freedom to manipulate the experimental conditions. An important factor is that the desired coherence transfer must take place under MAS conditions. This means that adiabatic passages can occur for most crystallites in a powder even if a modulated irradiation is used that creates two sidebands at fixed frequencies $\pm\omega_m$, as is the case for FAM. In the FAM sequence the variation of $\Delta\omega_m(t) = \omega_Q(t) - \omega_m$ describes the transition through resonance and determines the adiabaticity of the rotation-induced coherence transfer. For the DFS the process is similar with the sole exception that ω_m is time dependent as well. This means that $\Delta\omega_m(t) = \omega_Q(t) - \omega_m(t)$ determines the adiabaticity of the transfer; this parameter can be influenced not only by varying the spinning speed but also by changing the sweep rate of the DFS. In combination with the fact that these terms can add or subtract nonadiabatic spinning and sweeping can still lead to adiabatic passages. Figure 11a shows the energy level diagram in the modulation frame of a single crystallite under the combined effect of a DFS and magic angle spinning. The avoided level crossings, occurring simultaneously for the $|1\rangle \leftrightarrow |2\rangle$ and $|3\rangle \leftrightarrow |4\rangle$ transitions, are clearly witnessed. This leads to a pure conversion $I_x^{1-4} \rightarrow a \cdot I_x^{2-3}$ and $I_y^{1-4} \rightarrow a \cdot I_y^{2-3}$.

Even under on-resonance CW irradiation (RIACT) efficient triple- to single-quantum conversion takes place (*4, 21*). The energy level diagram in the rotating frame for CW irradiation in a spinning crystallite is presented in Fig. 11b. If during the duration of the RF irradiation a zero-crossing of the quadrupolar interaction occurs, triple- to single-quantum coherence transfer can occur very efficiently, albeit with an additional phase modulation due to the fact that at the crossing all transitions are coupled and not just the 1–2 and 3–4 subspaces as in FAM and the DFS. This additional phase modulation is orientation dependent and hampers the echo formation in the MQMAS experiment, thus adversely affecting the performance of the RIACT experiment (*22*).

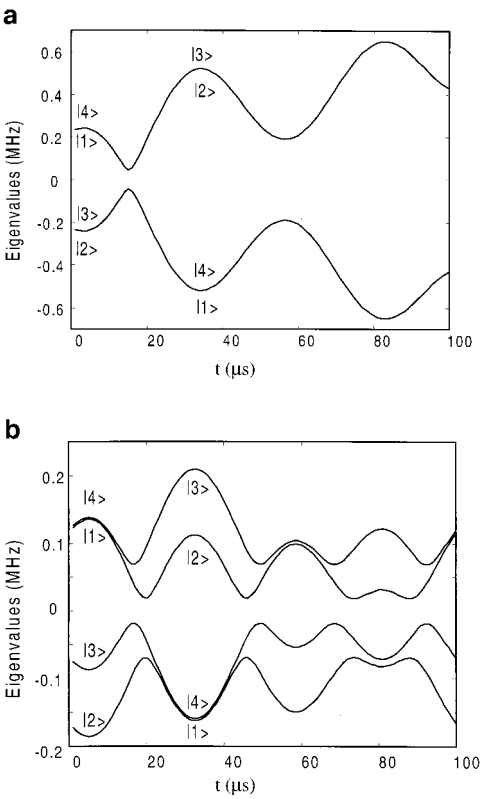

FIG. 11. Energy level diagram during magic angle spinning (MAS) for an $I = 3/2$ spin with $\Omega_Q/2\pi = 850$ kHz, $\eta = 0.1$, initial orientation $\alpha = 156°$; $\beta = 98°$; $\gamma = 12°$. (a) DFS from 0 to ± 1.3 MHz; (b) on-resonance CW irradiation during one rotor period ($\nu_1 = 50$ kHz, $\nu_r = 10$ kHz).

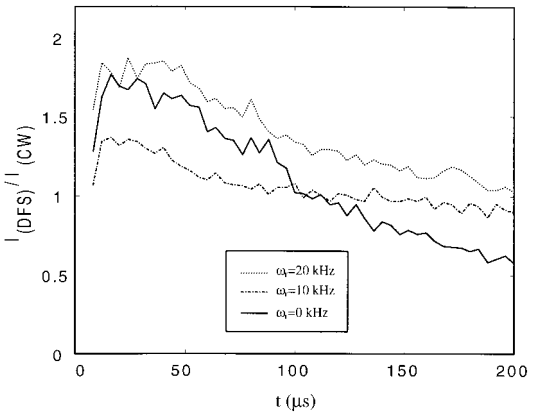

FIG. 12. 3Q to 1Q conversion process for powdered $NaNO_2$ (spinning at 0 (—), 10 (· – ·), or 20 (· · ·) kHz) using a short excitation pulse (ν_1 = 150 kHz) and DFS conversion. The sweep runs from 0 to 750 kHz with ν_1 = 80 kHz. The intensity is normalized with respect to the maximum intensity obtained with a two-pulse sequence employing an excitation and conversion pulse of 150 kHz.

The overall behavior of DFS, FAM, or RIACT in a powder is determined by the variation of the quadrupolar frequency during spinning. For optimum performance one strives to realize one single adiabatic passage for every crystallite in the powder. For the DFS we should follow the path of $\omega_Q(t) - \omega_m(t)$ during the excitation. In the powder each crystallite will have its own path. Therefore it will not be possible to reach the aforementioned truly adiabatic passage for every crystallite in the powder. So far our approach has been to optimize the performance of the DFS experimentally for the compound under study. A detailed account of adiabatic population and coherence transfer for static and spinning single crystals will be presented elsewhere (*36*).

An experimental verification of the 3Q → 1Q conversion process under a DFS as a function of sweep time is presented in Fig. 12 for powdered $NaNO_2$ spinning at 0 (static), 10, and 20 kHz. The intensity is normalized with respect to the maximum intensity obtained using the two-pulse experiment at an RF field strength of 150 kHz and an interpulse delay of 1 μs. The DFS ranged from 0 to 750 kHz and employed an RF field strength of 80 kHz. A first observation that can be made is that the DFS has a strong effect in the static sample. This implies that the DFS indeed induces the desired conversion for the majority of the crystals in the powder distribution, as the whole frequency range of the satellites is covered by the sweep. At a fixed modulation frequency, such as in FAM, only a limited number of crystallites with Ω_Q near ω_m would have been affected in a pulse-like fashion with the optimum conversion for the satellites experiencing an $N \cdot 180°$ pulse. Furthermore, the shape of the conversion curve, with a steep initial increase followed by a subsequent gradual decrease without any clear oscillatory behavior, is indicative that the process is indeed adiabatic. In fact the shape of the curves looks very similar to the curves obtained for population transfer (cf. Fig. 4). There, at elevated RF field strengths, the DFS also yielded the maximum efficiency for relatively short sweeps followed by a gradual decrease in efficiency with increasing sweep time. This similarity between population transfer and coherence transfer is in line with the theoretical description presented in the theory section. As is clear from Fig. 12, the curves for the spinning sample look very similar, again hinting at the adiabaticity of the process. Now the adiabaticity is determined by the combined effect of sweeping and spinning. The maximum signal gain is approximately 180% for the sample spinning at 20 kHz. Note that we compared the obtained signal gain of a DFS at 80 kHz with respect to a 150-kHz strong conversion pulse. If we had made the comparison with respect to an 80-kHz conversion pulse the signal gain amounts to more than 300%. The observed signal gain of a DFS compared to a conversion pulse will depend on the adiabaticity achieved with the DFS for the various crystallites in the powder and on the ratio ω_Q/ω_1 for the pulse. Pulse conversion is most efficient if the RF field strength is of the order of the quadrupolar frequency. In this regime the transitions in the quadrupolar spin system during a DFS are not well separated and its effect cannot be described as a consecutive passage of individual transitions. Numerical calculations are needed to calculate the results in this intermediate regime. An analytical approach with well-defined inversions of individual transitions demands that ω_1 is significantly smaller than ω_Q. The gain in performance of the DFS is expected to be most pronounced for samples with large quadrupolar interactions. The quantifiability, lineshapes, etc., of the MQMAS experiment employing DFS conversion, as a function of quadrupolar interactions and sweep parameters, are under investigation. This is aimed at developing a recipe giving reliable results for a maximum range of quadrupolar interactions.

Spin I = 5/2

For coherence transfer the spin-5/2 case is more complicated than the spin-3/2 case, as more transitions are involved and we have to consider 5Q and 3Q transfer to 1Q coherence separately. The energy level diagram of a spin 5/2 during a rotor period under on-resonance CW irradiation is shown in Fig. 13a. The most important feature of this diagram is that at the avoided level crossing the states $|1\rangle$ and $|6\rangle$ convert to the central transition states and vice versa. The states $|2\rangle$ and $|5\rangle$ are not involved in this transfer. This means that if the rotation takes place under adiabatic conditions, quintuple-quantum coherence is transferred to single-quantum coherence and vice versa. No triple- to single-quantum coherence takes place, however. Although a report of 3QMAS under RIACT conditions exists (*37*), the effects observed there cannot be called *rotationally induced adiabatic coherence transfer* in the strict sense of that formulation. Other coherence transfer mechanisms must be active. We have monitored 3Q → 1Q and 5Q → 1Q transfer under CW irradiation as a function of pulse length for the ^{27}Al resonance in powdered α-Al_2O_3. Clearly there is no

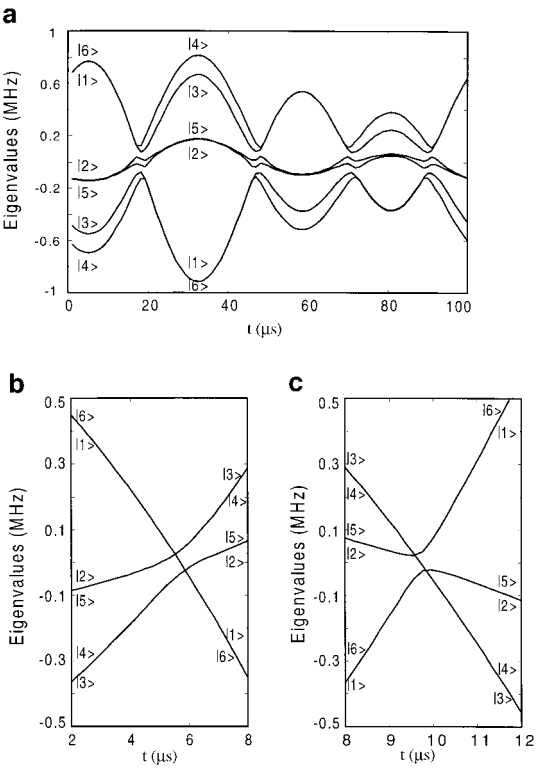

FIG. 13. Energy level diagram during magic angle spinning (MAS) for an $I = 5/2$ spin with $\Omega_Q/2\pi = 750$ kHz, $\eta = 0.1$, initial orientation $\alpha = 156°$; $\beta = 98°$; $\gamma = 12°$. (a) On-resonance CW irradiation during one rotor period. (b) DFS passage of the inner satellites and (c) passage of the outer satellites ($\nu_1 = 50$ kHz, $\nu_r = 10$ kHz).

RIACT effect for the triple- to single-quantum conversion (Fig. 14a); the intensity of a 3QMAS echo was monitored increasing the conversion pulse length from 0 to one full rotor period. After a peak obtained for the optimum conversion pulse length a gradual decrease in conversion efficiency is observed. In fact the conversion in a spinning sample soon drops below the conversion in a static sample. The performance for the 5QMAS echo is very different (Fig. 14b). For the rotating sample we observe the initial maximum for the optimum conversion pulse length followed by a steep decline; after a short time the efficiency of the conversion process increases again as the RIACT conversion starts to be effective for various crystallites in the powder distribution. A local maximum is reached at a quarter of a rotor period in accord with the predictions and observations of Vega (*21*) and Griffin and co-workers (*4*). The height of the RIACT maximum shown in Fig. 14b is slightly lower than the short pulse maximum. The relative height of these two maxima depends strongly on the ratio ω_Q/ω_1. Here we used a very strong RF field of 180 kHz so that ω_Q and ω_1 are of the same order of magnitude, in which case pulse excitation and conversion are rather efficient. If the RF field is relatively weak with respect to the quadrupolar interactions, RIACT conversion is more efficient as long as the zero crossing takes place adiabatically.

For the DFS the situation is different; now the inner and outer satellite transitions are traversed at different times. The energy level diagrams under the combined effect of a DFS and MAS are shown in Figs. 13b and 13c. For the coherence transfer this implies that we can transfer quintuple-quantum coherence to triple-quantum coherence to single-quantum coherence, but in the idealized situation ($\omega_1 \ll \omega_m, \Omega_Q$) no direct conversion from 5Q $\rightarrow$ 1Q conversion takes place. The latter transfer has to take place in two consecutive steps. For the 3Q $\rightarrow$ 1Q transfer we have to be aware that 3Q $\rightarrow$ 5Q transfer can take place as well. Therefore, it is advantageous to use diverging sweeps so that the inner satellites are traversed first. Furthermore, it is advantageous to avoid multiple crossings of the same transition as this may adversely influence the performance of the sweeps.

To experimentally support the argumentation presented above, we recorded the conversion efficiency for α-Al_2O_3 using the DFS ($\nu_1 = 115$ kHz). The intensity of the 3Q to 1Q conversion process as a function of the sweep time is presented in Fig. 15a for a sample spinning at 0, 10, and 20 kHz. The intensity is normalized with respect to maximum intensity obtained with a short conversion pulse with an RF field strength of 180 kHz, similar to the

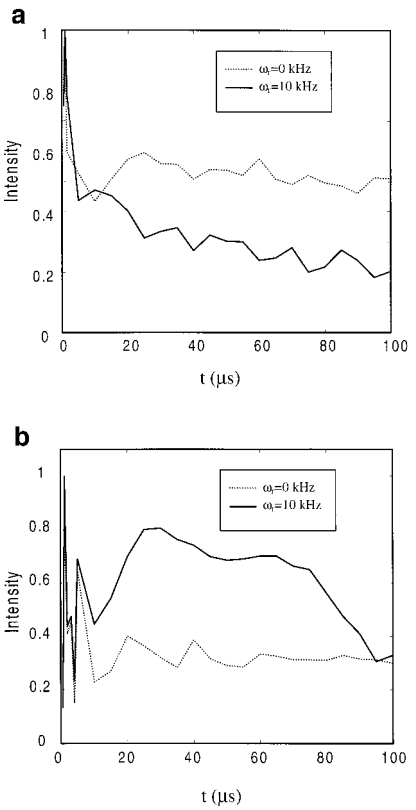

FIG. 14. MQ to 1Q coherence transfer under CW irradiation for powdered α-Al_2O_3. (a) 3Q to 1Q conversion ($\nu_1 = 150$ kHz) under static ($\cdots$) and 10 kHz (—) MAS (RIACT, $\alpha = 6.3$) conditions. (b) 5Q to 1Q conversion ($\nu_1 = 180$ kHz) under static ($\cdots$) and 10 (—) kHz MAS (RIACT, $\alpha = 9.1$) conditions. Only in the latter case is a clear RIACT maximum observed at 1/4 rotor period.

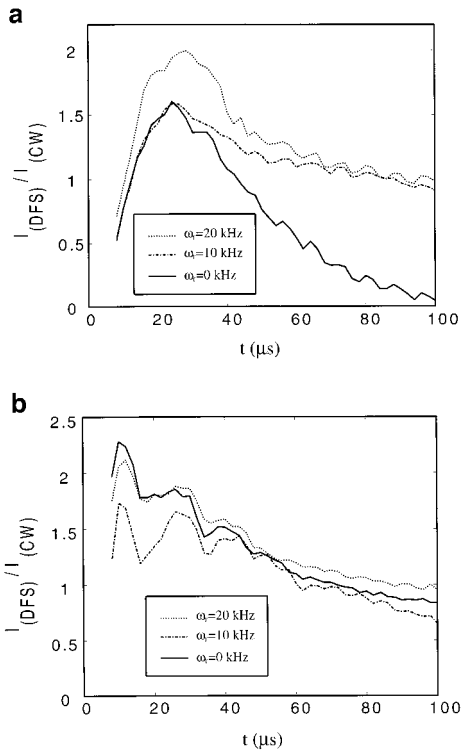

FIG. 15. MQ to 1Q coherence transfer for powdered α-Al_2O_3 (spinning at 0 (—), 10 (· – ·), or 20 (· · ·) kHz) using a short excitation pulse (ν_1 = 180 kHz) and DFS conversion. The sweep runs from 0 to 850 kHz with ν_1 = 115 kHz. The intensity is normalized with respect to the maximum intensity obtained with a two-pulse sequence employing an excitation and conversion pulse of 180 kHz. (a) 3Q to 1Q conversion. (b) 5Q to 1Q conversion.

situation in Fig. 14. As for the spin-3/2 case, the shape of curves suggests that the conversion is mainly achieved by the adiabatic process as fast oscillations, specific for the pulse-like conversion, are not present. Furthermore, we again observe a significant improvement for the static sample, which implies that the modulation of the Hamiltonian by the DFS is effective for many crystallites as the sweep covers the whole range of satellite frequencies in the powder. A gain of approximately 200% is obtained in conversion process for the sample spinning at 20 kHz. That the efficiency is the highest for the sample spinning at 20 kHz implies that there must either be an influence of the combined sweeping and spinning making the transitions more adiabatic or more crystallites experience an appropriate passage due to the combination. Again it must be considered that the reported gain is with respect to a pulse with significantly higher RF field strength than the DFS. As was already mentioned, pulse conversion depends on a mixing of states that is achieved when ω_1 and ω_Q are of the same order, whereas the adiabaticity concept using consecutive transitions demands that $\omega_1 \ll \omega_Q$. For relatively high ω_1 values the various subspaces are no longer isolated and the various transitions cannot be viewed independently. The effect of the DFS can then only be evaluated by a numerical approach.

The efficiency of the quintuple- to single-quantum conversion is plotted in Fig. 15b, using similar conditions as for the 3Q → 1Q transfer. Remarkably, a significant signal gain is again realized despite the fact that an idealized adiabatic DFS conversion has to proceed in two steps. Considering the strength of the RF field we cannot rule out that direct transfer of 5Q → 1Q coherence takes place for certain crystallites in the powder distribution that have a small Ω_Q at times that the modulation frequency is still small and not exceeding ω_1. For those sites a RIACT-type transfer will occur. Furthermore, "pulse-like" transfer can play a role. This would explain the oscillations we observe in the conversion curves. So in this case we do not argue that the conversion takes place mainly by a single well-described mechanism. More research is needed to clarify the relative importance of the different transfer processes.

3QMAS AND 5QMAS FOR SPIN I = 5/2

A good verification of the increased conversion efficiency of the DFS is obtained from the ^{27}Al 3QMAS whole-echo (*38*) spectrum of andalusite (Fig. 16). Andalusite has two different Al (I = 5/2) sites, a five-coordinated Al (C_{qcc} = 5.6 MHz, η = 0.76) and an octahedrally coordinated Al experiencing a very large quadrupolar interaction (C_{qcc} = 15.3 MHz, η = 0.13) (*39*, *40*). Alemany *et al.* (*40*) have recently shown the challenge that the latter site poses on the normal pulsed 3QMAS. Employing RF field strengths of up to 280 kHz, they were capable of making this site visible in a 3QMAS, albeit with a significantly distorted lineshape. For this site both the 3Q excitation and the 3Q → 1Q conversion are hampered. At the excitation side, one can increase the excitation pulse to a value above the recommended 180° pulse (*5*), which will further increase the excitation efficiency for the site with the large C_{qcc} whereas the intensity of the site with the smaller C_{qcc} will go down. The efficiency of the conversion process is the main problem, however. The effect of replacing this pulse by a DFS can be judged from Fig. 16. A diverging sweep from 0 to 2.5 MHz was employed using an RF field strength of 110 kHz; the spinning speed amounted to 25 kHz. As can be judged from Fig. 16b, a good signal to noise ratio is obtained, and more importantly the lineshape is in accord with the simulated shape without significant distortions. This absence of distortions is a further indication that most of the crystallites in the powder distribution must be affected by the DFS, not just a few with a favorable orientation.

The application of DFS-enhanced MQMAS spectra to "real" samples is demonstrated in a study of samples in the Al_2O_3–La_2O_3–B_2O_3 system prepared by sol-gel synthesis and subsequent heat treatment. Figure 17a shows the ^{27}Al MAS spectrum of a compound with overall composition $2Al_2O_3 \cdot 2La_2O_3 \cdot 4B_2O_3$ treated at 1100°C. The spectrum, obtained at 14.1 T spinning at 20 kHz, shows severe overlap and calls for MQMAS to resolve the various sites. In order to gain sensitivity and to obtain better lineshapes allowing a better extraction of the structural information, the conversion in the

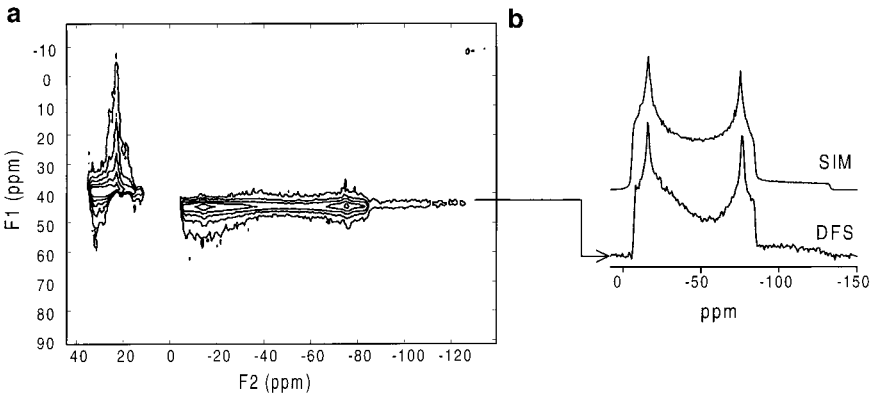

FIG. 16. DFS enhanced ^{27}Al 3QMAS whole-echo spectrum of andalusite using a 4.7-μs excitation pulse (ν_1 = 150 kHz) and a 12-μs-long DFS from 0 to $\pm$2.5 MHz (ν_1 = 115 kHz). The spinning speed was 20 kHz. 96 t_1 increments with an increment time of 8 μs were collected, acquiring 320 scans per experiment. (a) Contour plot showing the five- and sixfold coordinated Al. (b) The line of the Al(VI) (C_{qcc} = 15.3 MHz) is easily observed using moderate RF field strength and its shape appears to be hardly distorted.

3QMAS experiment, presented in Fig. 17b, is achieved by a DFS. We observe four well-resolved sites, a tetrahedrally coordinated aluminum, two fivefold coordinated Al species, and an octahedrally coordinated aluminum. The lineshapes of the fivefold coordinated Al both show distortions. The line marked Al(V)_1 lacks any clear features indicating a distribution in chemical shift and quadrupolar interaction, whereas the Al(V)_2 line shows clear singularities but is likely to be due to two overlapping lines. To further clarify this a 5QMAS experiment, again using DFS conversion, was carried out. The 5Q experiment, with different quadrupolar-induced shifts in the F_1 dimension, now clearly separates the Al(V)_2 into two different sites as is shown in the zoomed region of the 5QMAS spectrum presented in Fig. 18. Extraction of the quadrupolar parameters based on the quadrupolar induced shifts and the lineshapes in the 3QMAS spectra we come to the conclusion that the aluminum-bearing part of the compound consists of $9Al_2O_3 \cdot 2B_2O_3$ (A_9B_2) and a less well-crystallized phase

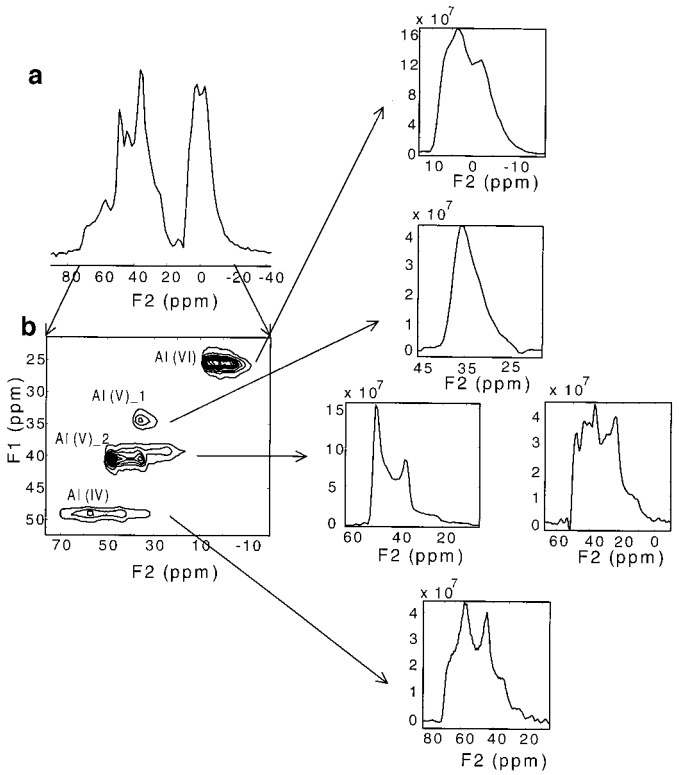

FIG. 17. DFS enhanced ^{27}Al 3QMAS whole-echo spectrum of $2Al_2O_3 \cdot 2La_2O_3 \cdot 4B_2O_3$ treated at 1100°C. 3Q to 1Q coherence transfer is enhanced with a 10-μs-long DFS from 0 to $\pm$2 MHz (ν_1 = 100 kHz). A strong (ν_1 = 180 kHz) 1.9-μs pulse is used for excitation. A spinning speed of 20 kHz was employed. (a) MAS spectrum. (b) 3QMAS spectrum.

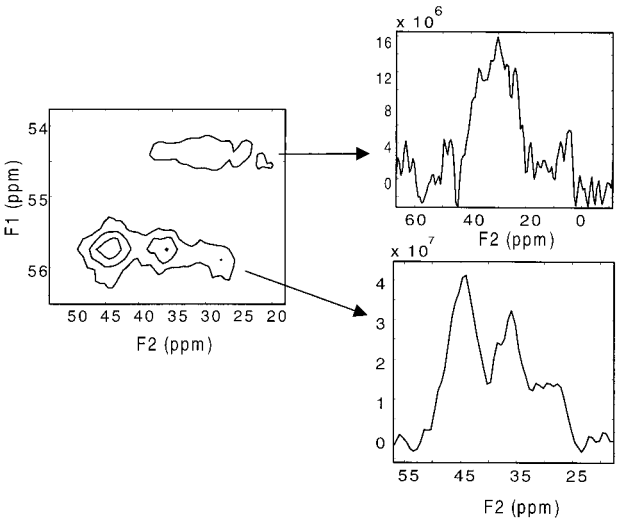

FIG. 18. Zoomed Al(V) region of the DFS enhanced ^{27}Al 5QMAS whole-echo spectrum of $9Al_2O_3 \cdot 2B_2O_3$. 5Q to 1Q coherence transfer is enhanced with a 12-μs-long DFS from 0 to 1.6 MHz at an RF field strength ν_1 = 140 kHz. In this spectrum the two sites overlapping in the resonance labeled Al(V)_2 in the 3QMAS spectrum of Fig. 17 are clearly separated.

containing mainly fivefold coordinated Al, giving rise to the Al(V)_1 signal. A full account of the study of these materials will be presented elsewhere.

Inspection of the lineshapes in the 5QMAS experiments shows strong distortions. Considering the fact that the quadrupolar coupling constants for Al in $9Al_2O_3 \cdot 2B_2O_3$ vary from 6 to 9 MHz (*41*), the excitation efficiency of the 5Q coherences is very low and will be partly selective. Furthermore, as was discussed in the previous section, different mechanisms are effective in the conversion. Idealized adiabatic DFS transfer will proceed in two steps, $5Q \rightarrow 3Q \rightarrow 1Q$, and thus both the outer and the inner satellites have to be traversed for this transfer to be effective; this cannot be realized for all crystallites in the powder. There will also be direct $5Q \rightarrow 1Q$ transfer, e.g., via a RIACT-type transfer for those crystallites for which ω_m is smaller than ω_1 when Ω_Q passes through zero. Finally, there will be excitation-type processes active. All the aforementioned processes will be effective for different crystallites with different efficiencies and might therefore lead to lineshape distortions.

CONCLUSIONS

Understanding the complex spin dynamics of half-integer quadrupolar nuclei under the combined action of sample rotation and CW or modulated RF irradiation is of utmost importance in designing more efficient experiments for these nuclei.

Pure amplitude modulation of the RF carrier leads to two sidebands placed symmetrically around the carrier frequency. By introducing a time dependence in this amplitude modulation, symmetric frequency sweeps can be generated. We have shown that these double frequency sweeps can be used to redistribute populations, by simultaneously inverting satellite transitions, in the spin system. This can be put to good use by transferring the population of the outer $|m\rangle$ and $|-m\rangle$ levels to the central $|1/2\rangle$ and $|-1/2\rangle$ levels prior to a selective excitation of the central transition. For single crystals this can lead to a signal gain of a factor of $2I$. It proved possible to approach this gain factor experimentally. For powders one has to compromise, as a distribution of quadrupolar frequencies exists; therefore it is not possible to fulfill the appropriate conditions for adiabatic population transfer in all crystallites. Experimentally we realized gain factors of 2.3 and 3 for $I = 3/2$ and $I = 5/2$ spin systems, respectively, demonstrating the usefulness of this concept for sensitivity enhancement for insensitive quadrupolar nuclei such as ^{17}O.

The DFS also proved to be an efficient tool for coherence transfer. When viewed from an appropriate modulation frame the dynamics of this coherence transfer proceeds in complete analogy to population transfer. The efficiency of $3Q \rightarrow 1Q$ coherence transfer was demonstrated for both $I = 3/2$ and $I = 5/2$ spin systems. Furthermore an effective $5Q \rightarrow 1Q$ transfer was achieved for spin $I = 5/2$ systems. This not only proves the $MQ \rightarrow 1Q$ coherence transfer to be much more efficient via a DFS, but also does so with significantly less RF power. Therefore DFS-enhanced MQMAS not only leads to improved signal to noise, but also extends the applicability of the experiment to sites experiencing quadrupolar interactions beyond the reach of the conventional pulsed method. Moreover, less distorted lineshapes are obtained in DFS-enhanced MQMAS experiments.

EXPERIMENTAL

All experiments were carried out on a Varian/Chemagnetics CMX Infinity 600 spectrometer, operating at 158.7 MHz for ^{23}Na and 156.3 MHz for ^{27}Al. Chemagnetics HX MAS probes of 2.5 and 3.2 mm were used, employing spinning speeds up to 25 kHz.

Double frequency sweeps were realized by a pure amplitude modulated carrier wave. Much attention was paid to avoid distortions of this modulation, as this would reintroduce on-resonance carrier, which will directly affect the spin system in an adverse way. To achieve a clean signal we use a commercially available, PC-based, arbitrary waveform generator from National Instruments (DAQArb PCI5411). This is used to generate the amplitude modulation on a center frequency of 14 MHz with a time resolution of 25 ns. This signal is added to the spectrometer frequency using a four-quadrant modulator to avoid distortions. The spectrometer frequency is set to 14 MHz below the desired frequency used to irradiate the nuclei under study so that the sum frequency is the (modulated) Larmor frequency (ω_0). This frequency is filtered and fed into the power amplifier in the usual way. The signal obtained from the sample is demodulated with an unmodulated 14 MHz before being fed into the receiver channel of the spectrometer. In this way all phase cycling capabilities, etc., from the spectrometer are retained, whereas we have great flexibility in generating waveforms. The waveforms used here are described by Eq. [6]. The starting frequency ω_s and the final frequency ω_f can be chosen freely so that both converging and diverging sweeps over any frequency range are possible.

ACKNOWLEDGMENTS

The authors are grateful to Prof. S. Vega for stimulating discussions and for supplying us with a preprint of his work on fast RF amplitude modulation (*22*). We wish to thank Mr. J. van Os, Mr. H. Janssen, Mr. G. Janssen, and Ms. G. H. Nachtegaal for their technical support. Ms. M. Brinksma is acknowledged for making her Mathematica NMR package available to us. We thank the Dutch foundation for chemical research NWO/CW for their financial support of this project.

REFERENCES

1. L. Frydman and J. S. Harwood, Isotropic spectra of half-integer quadrupolar spins from bidimensional magic-angle spinning NMR, *J. Am. Chem. Soc.* **117,** 5367–5368 (1995).
2. A. Medek, J. S. Harwood, and L. Frydman, Multiple-quantum magic-angle spinning NMR: A new method for the study of quadrupolar nuclei in solids, *J. Am. Chem. Soc.* **117,** 12779–12787 (1995).
3. G. Wu, D. Rovnyak, B. Sun, and R. G. Griffin, High-resolution multiple quantum MAS NMR spectroscopy of half-integer quadrupolar nuclei, *Chem. Phys. Lett.* **249,** 210–217 (1995).

4. G. Wu, D. Rovnyak, and R. G. Griffin, Quantitative multiple-quantum magic-angle-spinning NMR spectroscopy of quadrupolar nuclei in solids, *J. Am. Chem. Soc.* **118,** 9326–9332 (1996).
5. J. P. Amoureux, C. Fernandez, and L. Frydman, Optimized multiple-quantum magic-angle spinning NMR experiments on half-integer quadrupoles, *Chem. Phys. Lett.* **259,** 347–355 (1996).
6. J. P. Amoureux, C. Fernandez, and S. Steuernagel, Z filtering in MQMAS NMR, *J. Magn. Reson. A* **123,** 116–118 (1996).
7. C. Fernandez and J. P. Amoureux, Triple-quantum MAS-NMR of quadrupolar nuclei, *Solid State Nucl. Magn. Reson.* **5,** 315–321 (1996).
8. D. Massiot, Sensitivity and lineshape improvements of MQ-MAS by rotor-synchronized data acquisition, *J. Magn. Reson. A* **122,** 240–244 (1996).
9. D. Massiot, B. Touzo, D. Trumeau, J. P. Coutures, J. Virlet, P. Florian, and P. J. Grandinetti, Two-dimensional magic-angle spinning isotropic reconstruction sequences for quadrupolar nuclei, *Solid State Nucl. Magn. Reson.* **6,** 73–83 (1996).
10. S. P. Brown, S. J. Heyes, and S. Wimperis, Two-dimensional MAS multiple-quantum NMR of quadrupolar nuclei, removal of inhomogeneous second-order broadening, *J. Magn. Reson. A* **119,** 280–284 (1996).
11. S. P. Brown and S. Wimperis, Two-dimensional multiple-quantum MAS NMR of quadrupolar nuclei. Acquisition of the whole echo, *J. Magn. Reson.* **124,** 279–285 (1997).
12. M. J. Duer and C. Stourton, Further developments in MQMAS NMR spectroscopy for spin-3/2 nuclei, *J. Magn. Reson.* **124,** 189–199 (1997).
13. M. Hanaya and R. K. Harris, Optimization of two-dimensional multiple-quantum MAS NMR experiments for $I = 3/2$ nuclei on a moderate-field spectrometer, *J. Phys. Chem. A* **101,** 6903–6910 (1997).
14. J. P. Amoureux and C. Fernandez, Triple, quintuple and higher order multiple quantum MAS NMR of quadrupolar nuclei, *Solid State Nucl. Magn. Reson.* **10,** 211–223 (1998).
15. J. P. Amoureux, M. Pruski, D. P. Lang, and C. Fernandez, The effect of RF power and spinning speed on MQMAS NMR, *J. Magn. Reson.* **131,** 170–175 (1998).
16. S. W. Ding and C. A. McDowell, Shaped pulse excitation in multiquantum magic-angle spinning spectroscopy of half-integer quadrupole spin systems, *Chem. Phys. Lett.* **270,** 81–86 (1997).
17. S. W. Ding and C. A. McDowell, Multiple-quantum MAS NMR spectroscopy of spin-3/2 quadrupolar spin systems using shaped pulses spin systems using shaped pulses, *J. Magn. Reson.* **135,** 61–69 (1998).
18. L. Marinelli, A. Medek, and L. Frydman, Composite pulse excitation schemes for MQMAS NMR of half-integer quadrupolar spins, *J. Magn. Reson.* **132,** 88–95 (1998).
19. A. P. M. Kentgens and R. Verhagen, Advantages of double frequency sweeps in static, MAS and MQMAS NMR of spin $I = 3/2$ nuclei, *Chem. Phys. Lett.* **300,** 435–443 (1999).
20. P. K. Madhu, A. Goldbourt, L. Frydman, and S. Vega, Sensitivity enhancement of the MQMAS NMR experiment by fast amplitude modulation of the pulses, *Chem. Phys. Lett.* **307,** 41–47 (1999).
21. A. J. Vega, MAS NMR Spin locking of half-integer quadrupolar nuclei, *J. Magn. Reson.* **96,** 50–68 (1992).
22. P. K. Madhu, A. Goldbourt, L. Frydman, and S. Vega, Fast radio-frequency amplitude modulation in multiple-quantum magic-angle-spinning nuclear magnetic resonance: Theory and experiments, *J. Chem. Phys.* **112,** 2377–2391 (2000).
23. S. Vega and Y. J. Naor, Triple-quantum NMR on spin systems with $I = 3/2$ in solids, *J. Chem. Phys.* **75,** 75–86 (1981).
24. A. P. M. Kentgens, Quantitative excitation of half-integer quadrupolar nuclei by a frequency-stepped adiabatic half-passage, *J. Magn. Reson.* **95,** 619–625 (1991).
25. J. Haase, M. S. Conradi, C. P. Grey, and A. J. Vega, Population transfers for NMR of quadrupolar spins in solids, *J. Magn. Reson. A* **109,** 90–97 (1994).
26. J. Haase and M. S. Conradi, Sensitivity enhancement for NMR of the central transition of quadrupolar nuclei, *Chem. Phys. Lett.* **209,** 287–291 (1993).
27. E. van Veenendaal, B. H. Meier, and A. P. M. Kentgens, Frequency stepped adiabatic passage excitation of half-integer quadrupolar spin systems, *Mol. Phys.* **93,** 195–213 (1998).
28. R. Fu, V. L. Ermakov, and G. Bodenhausen, Divergent double chirp pulses for refocusing quadrupolar interactions, *Solid State Nucl. Magn. Reson.* **7,** 1–10 (1996).
29. S. Vega, Fictious spin 1/2 operator formalism for multiple quantum NMR, *J. Chem. Phys.* **68,** 5518–5527 (1978).
30. A. Wokaun and R. R. Ernst, Selective excitation and detection in multilevel spin systems; Application of single transition operators, *J. Chem. Phys.* **67,** 1752–1758 (1977).
31. J. Baum, R. Tycko, and A. Pines, Broadband and adiabatic inversion of a two-level system by phase-modulated pulses, *Phys. Rev. A* **32,** 3435–3447 (1985).
32. A. Abragam, "The Principles of Nuclear Magnetism," Oxford Univ. Press, Oxford, 1961.
33. M. M. Maricq and J. S. Waugh, NMR in rotating solids, *J. Chem. Phys.* **70,** 3300–3316 (1979).
34. G. Engelhardt, A. P. M. Kentgens, H. Koller, and A. Samoson, Strategies for extracting NMR parameters from 23Na MAS, DOR and MQMAS spectra. A case study for $Na_4P_2O_7$, *Solid State Nucl. Magn. Reson.* **15,** 171–180 (1999).
35. M. Edén and M. H. Levitt, Computation of orientational averages in solid-state NMR by Gaussian spherical quadrature, *J. Magn. Reson.* **132,** 220–239 (1998).
36. H. Schäfer, D. Iuga, R. Verhagen, and A. P. M. Kentgens, Population and coherence transfer in half-integer quadrupolar spin systems in static and spinning single crystals driven by double frequency sweeps, *J. Chem. Phys.,* in press (2000).
37. T. Mildner, M. E. Smith, and R. Dupree, Rotationally induced triple quantum coherence excitation in MAS NMR spectroscopy of $I = 5/2$ spins, *Chem. Phys. Lett.* **301,** 389–394 (1999).
38. P. J. Grandinetti, J. H. Baltisberger, A. Llor, Y. K. Lee, U. Werner, M. A. Eastman, and A. Pines, Pure-absorption-mode lineshapes and sensitivity in 2-dimensional dynamic-angle spinning NMR, *J. Magn. Reson. A* **103,** 72–81 (1993).
39. R. Dupree, I. Farnan, A. J. Forty, S. El-Mashri, and L. Bottyan, A MAS NMR study of the structure of amorphous alumina films, *J. Physique C* **12,** C8 113–117 (1985).
40. L. B. Alemany, S. Steuernagel, J. P. Amoureux, R. L. Callender, and A. R. Barron, Very fast MAS and MQMAS NMR studies of the spectroscopically challenging minerals kyanite and andalusite on 400, 500, and 800 MHz spectrometers, *Solid State Nucl. Magn. Reson.* **14,** 1–18 (2000).
41. D. Massiot, D. Muller, T. Hubert, M. Schneider, A. P. M. Kentgens, B. Cote, J. P. Coutures, and W. Gessner, Double rotation and magic-angle spinning nuclear magnetic resonance study of Al-27: Reexamination of the aluminium borate $9Al_2O_3 \cdot 2B_2O_3$, *Solid State Nucl. Magn. Reson.* **5,** 175–180 (1995).